Candidate Compounds for the Chemoprevention of Hereditary Diffuse Gastric Cancer

Emily Schulpen

A thesis submitted in partial fulfilment of the degree:
Bachelor of Biomedical Sciences with Honours

Department of Biochemistry
University of Otago, Dunedin, New Zealand

October 2019

Abstract

Hereditary diffuse gastric cancer (HDGC) is a cancer syndrome caused by germline mutations in the tumour suppressor gene *CDH1*, which encodes the cell-cell adhesion protein E-cadherin. Mutations in *CDH1* lead to increased proliferation, invasiveness and loss of cell polarity. Patients with germline *CDH1* mutations have a 70% lifetime risk of developing gastric cancer. Female carriers also have a 42% lifetime risk of developing lobular breast cancer.

The current optimal treatment for HDGC is a prophylactic gastrectomy as surveillance through endoscopy is imperfect and tumours can be discovered at a late stage. This project aims to utilise the synthetic lethal (SL) approach to find a chemopreventative treatment for HDGC. The SL approach aims to manipulate cell viability by exploiting the relationships between related genes. Synthetic lethality is a gene relationship in which an inactivation of either of two genes alone allows cell survival, however when both are inactivated it leads to cell death.

Previous work within the laboratory has identified potential SL targets for *CDH1* via high throughput drug screening. This was carried out in an isogenic pair of non-tumourigenic breast epithelial MCF-10A cell lines, one lacking *CDH1* function. This identified histone de-acetylase inhibitors (HDACi) and statins as promising SL therapies for HDGC as they can selectively inhibit growth of $CDH1^{-/-}$ cells. Epigenetic changes, such as histone acetylation and deacetylation, modify expression patterns and are linked to cancer progression. Statins are widely used, well tolerated drugs that lower cholesterol levels and impact on plasma membrane organisation.

This project has validated successful SL compounds from the MCF-10A drug screen in a gastric cancer model, using isogenic NCI-N87 *CDH1*$^{+/+}$ and *CDH1*$^{-/-}$ cell lines. Promising compounds that have shown the best SL effect in 2D cell culture models, were then analysed for clinical trial data to find drugs that have minimal adverse effects. The compounds with minimal side effects and strong SL relationship with *CDH1*, were then assessed in a gastric organoid model of HDGC. This organoid model called the air-liquid interface (ALI) model, is a 3D representation of the gastric gland and contains all gastric cell lineages. As such it is a more accurate pre-clinical model for drug screening than 2D cultures. A second organoid model, the submerged model, was also further developed as it is a higher throughput model and will be more efficient for future drug compound testing. Mocetinostat, the compound identified to have the best synthetic lethal effect, will now undergo further preclinical testing as a potential chemopreventative compound for families affected by HDGC.

Acknowledgements

I would firstly like to thank my supervisor Professor Parry Guilford for all your support and guidance during this project. Your passion for the SL project is inspiring and I have really enjoyed being a part of the lab this year!

Thanks to the SL group, everyone has been incredibly helpful and great to work with, special thanks to Tom - you have been so amazing. Thanks for answering all my questions and also for letting me join you in setting up the submerged organoids! I owe you a few more 8 hour TC sessions ☺ Also thanks to the whole CGL group, you have all made the lab a really great place to be. I will miss working with you guys and the always random tea room discussions.

Thanks to the London girls, you guys never fail to make me laugh and have made this year so much fun and have been so supportive, couldn't have done it without you *peace

Thanks to my family for the constant support, for coming to visit me and for always being free for a chat. Your enthusiasm for what I'm doing is the best, keep sending me every single cancer related article/video/LinkedIn post you see – I love it!

Lastly, special thanks to the HDGC whānau, it was incredibly motivating meeting some of you this year, I hope this project has taken the research a step further.

Table of Contents

Abstract 1

Acknowledgements 3

Table of Contents 4

Abbreviations 7

List of Figures 9

List of Tables 9

Chapter 1: Introduction 10

1.1 Gastric cancer 10

1.1.1.Gastric cancer in New Zealand 11

1.1.2.Histological subtypes of gastric cancer 11

1.2. Hereditary Diffuse Gastric Cancer 13

1.2.1. E-cadherin 14

1.2.1.1. Pathogenic E-cadherin 15

1.2.1.2. E-cadherin and HDGC 16

1.2.2. Treatment and prevention of HDGC 16

1.2.2.1.Prophylactic Gastrectomy 17

1.2.2.2. Endoscopic surveillance 17

1.3. Synthetic lethality 18

1.3.1. Drug candidates for HDGC treatment 19

1.3.1.1. Statins 20

1.3.1.2. Histone De-acetylase inhibitors 20

1.4. Current models of gastric cancer 22

1.4.1. Cell culture model 22

1.4.2. Gastric organoid models 22

1.4.2.1. Air liquid interface model 23

1.4.2.2. Submerged model 24

1.4.2.3. Additional models 24

1.4.3 Mouse models 24

1.5. Aims 25

Chapter 2: Materials 26

2.1 List of Reagents 26

2.2 List of Equipment 27

2.3 Software 28

2.4 Ethics 28

Chapter 3: Methods 29

3.1. NCI-N87 culture 29

3.1.1. Resurrection of NCI-N87 cells 30

3.1.2. Cryogenic preservation of NCI-N87 cells 30

3.1.3. NCI-N87 drug screening 30

3.1.3.1. 24 hour edge count 31

3.1.3.2. Cell viability assay 32

3.1.3.3. Statistical analysis 32

3.2. Air-liquid interface Organoid model 32
3.2.1. Myofibroblast culture 32
3.2.1.1 Passage 33
3.2.1.2 MFB11 Resurrection 33
3.2.1.3. Cryogenic preservation 34
3.2.2. Air-Liquid Interface Organoid Drug assay preparation 34
3.2.2.1. MFB co-culture preparation 34
3.2.2.2 Organoid culture 34
3.2.2.2.1. Collagen preparation: *Base Layer* 34
3.2.2.2.2 Mouse Euthanasia and stomach extraction 35
3.2.2.2.3 Collagen preparation: *Tissue layer* 37
3.2.2.2.4 Induction of *CDH1* knockout 38
3.2.3. ALI drug screening 39
3.2.3.1.Quantification of ALI organoid viability 39
3.2.3.2. Statistical analysis 40
3.2.4 ALI-halo Organoid Analysis 41

3.3. Submerged Organoid model 41
3.3.1. Organoid preparation from primary tissue 42
3.3.1.1. Stomach extraction 42
3.3.1.2. Gastric gland isolation and seeding 42
3.3.2. Media components 43
3.3.3. Submerged organoid culture 44
3.3.3.1. Submerged organoid passage 45
3.3.4. Submerged organoid drug screening 46
3.3.4.1. CDH1 knockout Induction 47
3.3.4.2. Drug addition 47
3.3.4.3. Viability assay 47
3.3.5. Cryogenic preservation 48
3.3.6. Resurrection of submerged organoids 48

Chapter 4: Results 50

4.1 NCI-N87 drug assay data 50
4.1.1. Atorvastatin 50
4.1.2 Histone Deacetylase inhibitors 51
4.1.2.1 Entinostat 51
4.1.2.2. Pracinostat 52
4.1.2.3. Mocetinostat 53
4.1.2.4. Vorinostat 54

4.2. ALI Organoid data 55
4.2.1. ALI drug screening 56
4.2.1.1. Vorinostat 57
4.2.1.2. Mocetinostat 58
4.2.2. 'Halo' organoids 61
4.2.2.1 Identification of Halo organoids 61
4.2.2.2. Halo organoid analysis 64

4.3. Submerged organoid data: 65
4.3.1. TGFßi addition to growth media 66
4.3.2. Seeding density analysis 68
4.3.3 DMSO toxicity 70
4.3.4 Preliminary submerged model drug assay 71

4.4. Concluding remarks 73

Chapter 5: Discussion 74

5.1 Identification of SL compounds 74

5.1.1 Vorinostat 74
5.1.2. Mocetinostat 75
5.2. Limitations 77
5.2.1 NCI-N87 model 77
5.2.2. ALI model 78
5.2.3 Submerged 79
5.3 Future directions 81
5.4. Clinical relevance 83
5.5 Concluding statement 84
Appendix 85

Abbreviations

% - Percent

°C – Degrees Celsius

µg – Microgram

µL – Microlitre

µm – Micrometre

µM – Micromole(s) per litre

2D – Two dimensional

3D – Three dimensional

ALI – Air liquid interface

CDH1 – E-cadherin

cm – centimetre

CO_2 - Carbon dioxide

CTCL – Cutaneous T-cell lymphoma

DAPI – 4′,6-diamidino-2-phenylindole

DGC – Diffuse gastric cancer

DMEM-F12 – Dulbecco's modified Eagle's medium and F12 medium

DMSO – Dimethyl sulfoxide

EMT – Epithelial-mesenchymal transition

FBS – Foetal bovine serum

FITC - Fluorescein isothiocyanate

HDACi – Histone deacetylase inhibitor

HDAC – Histone deacetylase

HDGC – Hereditary Diffuse Gastric Cancer

HMG-CoA – 3-hydroxy-3-methylglutaryl-coenzyme A

iPSC – Induced pluripotent stem cell

KO – Knockout

LN_2 – Liquid nitrogen

MFB11 – Myofibroblast cell line

mL – Millilitre(s)

mm^3 – Millimeters cubed

mM – Millimole(s) per litre

PARP - Poly (ADP-ribose) polymerase

PBS – Phosphate buffered saline

PFA – Paraformaldehyde

RCF – Relative Centrifugal Force

SC – Stem cell

SL – Synthetic lethality

WT – Wildtype

List of Figures

Figure 1: Primary gastric cancer histological subtypes according to Lauren classification. 12
Figure 2: Schematic of the adherens junction. 15
Figure 3: Schematic of synthetic lethality. 19
Figure 4: 96 well plate plan for NCI-N87 drug assay. 31
Figure 5: Diagram of ALI organoid drug assay preparation. 38
Figure 6: Diagram of well conditions for ALI organoid drug assay. 39
Figure 7: Normalised nuclei counts 48 hours post treatment with a serial dilution of Atorvastatin. 51
Figure 8: Normalised nuclei counts 48 hours post treatment with a serial dilution of Entinostat. 52
Figure 9: Normalised nuclei counts 48 hours post treatment with a serial dilution of Pracinostat. 53
Figure 10: Normalised nuclei counts 48 hours post treatment with a serial dilution of Mocetinostat. ..54
Figure 11: Normalised nuclei counts 48 hours post treatment with a serial dilution of Vorinostat. 55
Figure 12: Representative brightfield images of Air-Liquid interface (ALI) organoids treated with DMSO (control), Vorinostat and Mocetinostat. 60
Figure 13: Percentage change in growth analysis of ALI organoids treated with Vorinostat and Mocetinostat. 61
Figure 14:Comparative image of a true organoid compared to a 'halo' organoid. 62
Figure 15: Representative images of halo degradation in 5µM Vorinostat treated ALI organoids. 63
Figure 16: ALI halo organoid integrity blinded analysis. 65
Figure 17: Submerged organoids treated with and without TGFß inhibitor. 68
Figure 18: Representative images of submerged organoid seeding density analysis. 70
Figure 19: Submerged organoid DMSO toxicity assay. 71
Figure 20: Submerged organoids pilot drug assay with Mocetinostat 72

List of Tables

Table 1: Concentration of components in CellMatrix™ collagen gel culturing kit for culture of the ALI organoid model 35
Table 2: Complete growth medium for submerged organoids 44
Table 3: Basal medium for submerged organoid passage 44
Table 4: Submerged organoid freezing medium 48

Chapter 1: Introduction

1.1 Gastric cancer

Gastric cancer has the fifth highest incidence of all cancers worldwide, and the third highest mortality rate [2]. 783,000 deaths were due to gastric cancer in 2018, this is 75% of the number of new cases diagnosed that year [3]. The high mortality rate is due to gastric cancer being: i) relatively asymptomatic in mid stages and ii) a multifactorial disease with many environmental and genetic risk factors. This culminates in late stage detection of gastric cancer and poor prognosis for patients with a 5-year survival rate of 10% [4].

Gastric cancer rates vary with geographical location, with the highest incidence of 22.4 cases per 100,000 people in East Asia, while the lowest incidence occurs in Western Europe with an incidence of 5.8 in 2018 [3]. This regional variance is due to different exposures to environmental risk factors, like high salt diets, smoking, obesity and *Helicobacter pylori (H. pylori)* infection rates [5, 6]. *H. pylori* usually presents as an asymptomatic infection with around 44.3% of the population being carriers [7] and around 5% of these carriers will develop gastric cancer, making it the most penetrant environmental risk factor [8]. The incidence of gastric cancer worldwide is two-fold higher in males than females [3]. Studies show that oestrogen may have a protective effect in *H. pylori* induced gastric cancer, leading to the lower incidence in females [9].

The global incidence of gastric cancer has decreased overtime due to the mitigation of environmental risk factors through improved food preservation, diet and reduced rates of *H. pylori* infection [10, 11]. However, there are also genetic risk factors for gastric cancer, for example mutations in the *CDH1* gene. Genetic risk does not fluctuate like environmental risk

factors, therefore the incidence of gastric cancer in the younger population has stayed constant [12].

1.1.1.Gastric cancer in New Zealand

New Zealand (NZ) is a relatively low incidence country, with mortality rates of less than 4 per 100,000 people, compared to over 20 in countries in East Asia [6, 7, 13, 14]. In NZ, the rates of gastric cancer are disproportionately high in the Māori and Pacific populations, with a three- to six-fold increase in the rate of gastric cancer compared to NZ European populations [8]. A study by Ellison-Loschmann *et al*. showed that the NZ Māori population had an increased exposure to environmental risk factors, for example rates *H. pylori* infection and smoking. This may partially explain the increased prevalence of gastric cancer [15]. Similar to worldwide statistics, the incidence and mortality rate of gastric cancer in NZ is decreasing [16].

1.1.2.Histological subtypes of gastric cancer

There are two primary histological subtypes of gastric adenocarcinoma, intestinal- and diffuse-type, as defined by the Lauren classification. There are also mixed histologies of the two subtypes, and some adenocarcinomas are not able to be defined within the Lauren classification [17]. Intestinal-type gastric cancer presents with intestinal metaplasia, well-defined gastric ducts, inflammatory infiltrate and larger tumour cells with enlarged pleomorphic nuclei (Figure 1A) [13, 17]. In contrast, diffuse-type consists of isolated tumour cell groups lacking glandular structure, partially due to the lack of cell-cell junctions [14, 18]. Diffuse-type is often comprised of signet ring cells. Signet ring cells are large cells with mucous filled vacuoles that push the nucleus to the periphery (Figure 1B). However, signet

ring cells are not limited to diffuse-type adenocarcinomas and can be found in intestinal-type lesions, but less frequently [13].

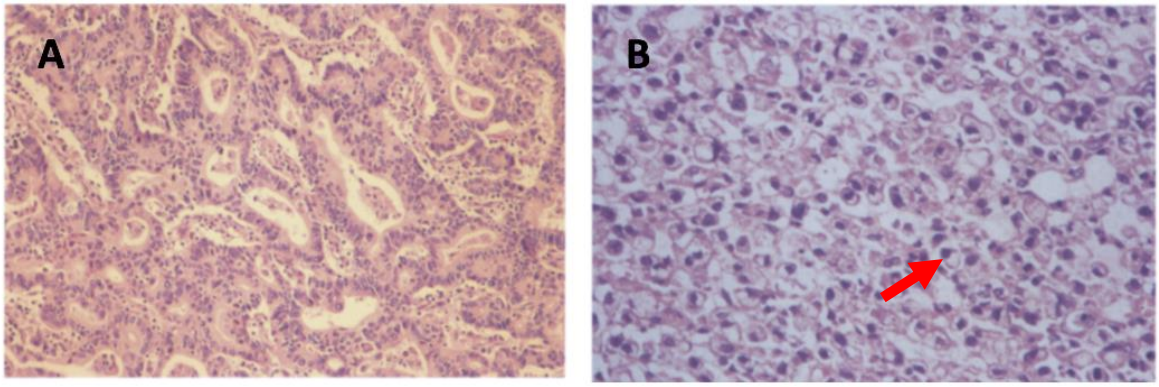

Figure 1: Primary gastric cancer histological subtypes according to Lauren classification. *A: Intestinal-type gastric cancer with defined gastric ducts B. Diffuse-type gastric cancer with lack of glandular structure and large numbers of signet ring cells (Arrow pointing to a signet ring cell). Excerpt from [19].*

Another key histological classification system is the World Health Organisation (WHO) classification which defines 4 major gastric cancer subtypes and many uncommon variants. Tubular adenocarcinoma is the most common major subtype, presenting as large polyploid branching tubules surrounded by nuclear and inflammatory debris. Papillary adenocarcinoma subtype consists of epithelial projections held together by a fibrovascular centre. Mucinous adenocarcinoma is the third WHO subtype, accounting for 10% of gastric carcinomas. Mucinous adenocarcinoma is histologically characterised by glandular or clustered cells, surrounded by extracellular mucous pools, which make up over 50% of the tumour mass. Lastly, signet ring cell carcinoma, or poorly cohesive subtype, contains a mixture of signet ring cells and other non-signet ring cells. These can form irregular cell structures similar to glands and micro-trabeculae[20]. The signet ring cell carcinoma subtype correlates with the Lauren classification of diffuse-type gastric cancer [20] and the Lauren classification of intestinal-type correlates with the papillary, tubular and mucinous WHO subtypes [21].

The Cancer Genome Atlas (TCGA) has developed a molecular classification system, identifying four molecular subtypes; Epstein-Barr virus (EBV) infected tumours, tumours with microsatellite instability (MSI), genomically stable (GS) tumours and tumours with chromosomal instability (CIN) [22]. The CIN molecular subtype comprised 50% of the total samples and presented with aneuploidy, gene amplifications and *TP53* mutations. The histology of the CIN subtype showed glandular structure and correlated with the Lauren intestinal-type gastric cancer. The Lauren diffuse-type histology was seen in the TCGA GS subtype, which composed 20% of the total samples and had the largest proportion of *CDH1* mutations [23]. However, this classification of histological (Lauren and WHO) or molecular (TCGA) subtype is currently a descriptive tool that is unable to provide any prognostic information. Understanding of the molecular subtypes is essential for the development of targeted molecular therapies, but histological or molecular subtype currently has no impact on treatment stratification and all gastric cancers are treated uniformly [22, 23].

1.2. Hereditary Diffuse Gastric Cancer

1-3% of all gastric cancer cases are due to a genetic predisposition [24]; Hereditary Diffuse Gastric Cancer (HDGC) makes up one third of this group [24]. HDGC was first discovered in 1998 in a Māori whānau with a family history of gastric cancer. These family members presented with diffuse-type gastric cancer, and suffered a mortality age ranging from 14-40 years old, in contrast with the NZ mean age of over 60 years [25]. A mutation in *CDH1* was found to be the cause of the hereditary gastric cancer [25]. In NZ Māori, 13% of all diffuse gastric cancer cases are due to a mutation in *CDH1*, this is three to five fold higher than that of the NZ European population. *CDH1* mutations are therefore an important contributor to the increased rate of gastric cancer in the Māori population [26].

HDGC is an autosomal dominant syndrome caused by germline mutations in the *CDH1* gene encoding the cell adhesion protein E-cadherin. Mutations in *CDH1* lead to a 70% lifetime risk of developing diffuse gastric cancer in men and 56% for women [27]. The lifetime risk of developing lobular breast cancer also increases to 42% for women [27]. The histological subtype of HDGC is the Lauren diffuse-type, with pagetoid spread (proliferation of cells between the epithelia and basement membrane) of signet ring cells amongst the normal mucosal layer of the gastric epithelia [27]. The discovery of the molecular mechanism has led to early diagnosis of more people and an understanding of the disease [14, 25, 28, 29] but no prophylactic drug treatments currently exist. Further investigation into the molecular mechanism therefore needs to occur to improve treatment options for patients.

1.2.1. E-cadherin

The *CDH1* gene encodes the cell adhesion protein E-cadherin, which belongs to the cadherin superfamily of transmembrane glycoproteins[12, 30, 31]. E-cadherin has an important role in cell structure [30] as it is an integral part of the adherens junction (Figure 2). Extracellular domains of adjacent E-cadherin molecules form homodimers, allowing connection to the intracellular actin cytoskeleton between adjacent cells (Figure 2). This connection of E-cadherin to the intracellular actin cytoskeleton occurs through alpha and ß-catenin molecules [32]. The adherens junction made up of E-cadherin homodimers form dynamic strong bonds between neighbouring cells to maintain individual cell structure.

As well as maintaining cellular and tissue structure, the adherens junctions between epithelial cells also directs correct cell polarity. This is important for the orientation of the mitotic spindle, and the resulting division of daughter cells within the epithelial plane [33]. E-cadherin is also involved in cellular signalling through interaction with ß-catenin, a key part

of the WNT signalling pathway. E-cadherin holds ß-catenin at the cytoskeleton, preventing its translocation to the nucleus where it activates gene transcription [32].

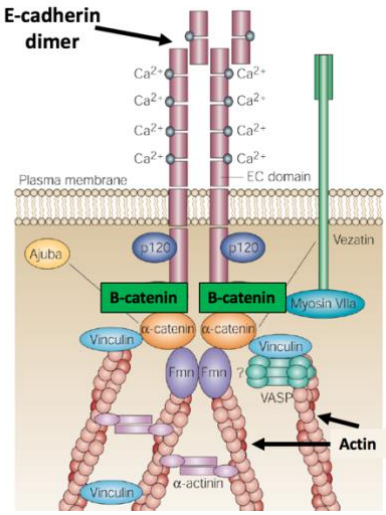

Figure 2: Schematic of the adherens junction.
Adherens junction between two epithelial cells highlighting the E-cadherin homodimer and interactions between E-cadherin, ß-catenin and Actin. Adapted from Kobielak et al. [1]

1.2.1.1. Pathogenic E-cadherin

CDH1 mutations leading to inactivation of E-cadherin are associated with increased invasiveness and metastasis, abnormal differentiation and proliferation, and loss of both cell adhesion and cytoskeletal organisation[34]. This is due in part to the lack of adherens junctions and in turn the inability to maintain cell polarity. This allows for mis-alignment of the mitotic spindle and mitosis to occur out of the epithelial plane, resulting in increased invasion into other tissue and abnormal cell differentiation[33]. Loss of E-cadherin function is also a key step in inducing Epithelial to Mesenchymal transition (EMT) which is the process where epithelial cells transition towards a mesenchymal cell phenotype. EMT is a normal process in embryonic development, however, in cancer, this process is associated with increased invasiveness and metastasis [35]. All of these factors mean *CDH1* is an important tumour suppressor gene in epithelial cells, and loss of *CDH1* function leads to cancer development [36].

1.2.1.2. E-cadherin and HDGC

A third of all hereditary gastric cancers are due to germline mutations in the *CDH1* tumour suppressor gene [24]. Germline homozygous loss of function of *CDH1* is embryonically lethal [37], so HDGC patients have one mutated *CDH1* allele and have heightened sensitivity to mutation or epigenetic silencing of the second wild type *CDH1* allele, triggering the development of gastric cancer [38]. Mutation of the second *CDH1* allele leads to the loss of E-cadherin, causing all the pathogenic effects discussed previously: loss of cell adhesion, loss of cell polarity, increased proliferation, invasion into mucosal tissue, leading to the formation of signet ring cell carcinomas and HDGC. There have been over 155 different germline *CDH1* mutations identified, 126 of which being pathogenic and the remainder unclassified [39]. These different *CDH1* mutations are found throughout the whole gene, with no evidence of phenotype-genotype correlation, meaning all *CDH1* mutation positive gastric cancers are clinically treated the same [39].

1.2.2. Treatment and prevention of HDGC

Clinical guidelines for the treatment of HDGC have developed from the improved knowledge of the syndrome and the role of *CDH1* in the penetrance of gastric cancer. Current clinical guidelines recommend that patients who fulfil any of the following criteria should undergo genetic testing for a pathogenic *CDH1* mutation[27].

- Two cases of gastric cancer in the family, regardless of age, with one confirmed as a diffuse subtype gastric cancer.
- One case of diffuse-type gastric cancer in a family member under 40 years of age.
- Family history of diffuse gastric cancer and lobular breast cancer, with at least one case prior to 50 years of age.

After genetic screening, if a pathogenic *CDH1* mutation is found, patients have two treatment options: endoscopic surveillance or prophylactic gastrectomy. Genetic counselling is also provided alongside this process to guide patients through their diagnosis and the risks and benefits of each treatment option[12].

1.2.2.1.Prophylactic Gastrectomy

If a pathogenic *CDH1* mutation is found, the recommended treatment is prophylactic gastrectomy, which is the complete resection of the stomach[27]. Prophylactic gastrectomy has a large impact on life post-surgery, as there are psychological and physiological impacts on the patient that need to be monitored. Patients can suffer from weight loss, nutrient deficiencies and loss of appetite[27]. However, >96% of gastrectomy samples contain subclinical signet ring cell carcinomas. These microscopic cancerous lesions would have likely developed into advanced diffuse gastric cancer. Therefore, despite the significant side effects, prophylactic gastrectomy clearly eliminates the risk of disease progression[40]. However, the morbidity associated with prophylactic gastrectomy highlights the need for new, less invasive treatments for these families.

1.2.2.2. Endoscopic surveillance

Another management option is screening or surveillance through endoscopy. Screening relates to patients who are not aware of their *CDH1* mutation status and surveillance for patients who carry a *CDH1* mutation, but have decided to not have a prophylactic gastrectomy *[27].* Detection of HDGC through endoscopy is difficult, as the cancer spreads through the mucosal layer under the gastric epithelia, making it hard to detect visually [27]. Signet ring cell foci often appear as slight discolouration or pale areas in the epithelia [27]. Therefore endoscopy is not the recommended management strategy, as it does not eliminate

the risk of developing HDGC. Patients who choose to undergo endoscopic surveillance are occasionally only diagnosed at a late stage, when foci become more visible, leading to poor prognosis and a less than 10% five year survival rate [4]. The only current effective treatment to remove all risk of HDGC is a prophylactic gastrectomy. A chemopreventative therapy needs to be developed to reduce the need for gastrectomy and the risk of developing HDGC.

1.3. Synthetic lethality

Synthetic lethality is an interaction between two genes where as long as one of the two genes is functional, the cell is viable. However when function in both genes is lost simultaneously, the effect is lethal (Figure 3)[41]. This synthetic lethal (SL) relationship was first discovered in *Drosophila.* Certain chromosomes were 'synthetic-' or 'semi-lethal' when inherited together, producing non-viable offspring, but viable when inherited separately[42]. These gene relationships occur naturally to ensure redundancy in cellular processes, so that function in a single gene isn't required for viability, thus reducing the impact of mutation[43]. Mutations in tumour suppressor genes in cancer can potentially be exploited through targeting of their synthetic lethal partner genes. Using this approach, cancer cells with characteristic mutations in tumour suppressor genes can be specifically targeted, leaving healthy cells relatively unharmed[44]. This approach has been used in relation to cancers with *BRCA1/2* mutations. PARP inhibitors induce an SL phenotype and fully inhibit the DNA repair pathway, meaning cancer cells with *BRCA* mutations are no longer viable [45, 46].

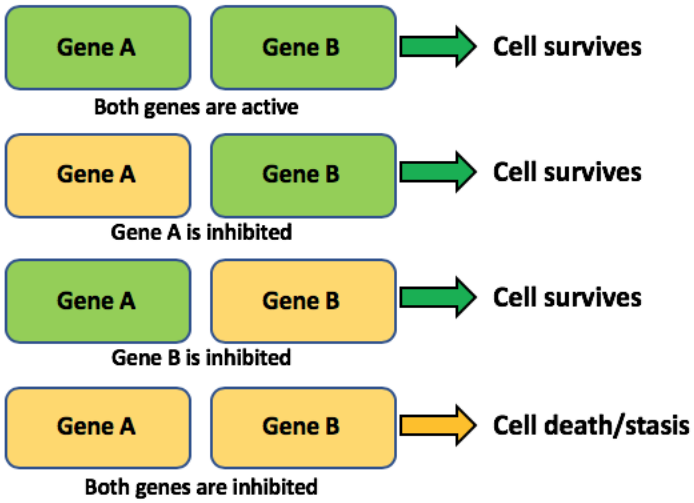

Figure 3: Schematic of synthetic lethality.
Gene A and B are synthetic lethal partner genes. When function is lost in one synthetic lethal partner gene the cell survives. Loss of function in both synthetic lethal partners genes leads to cell death.

This synthetic lethal strategy provides a promising approach for the development of novel therapies for HDGC, through targeting genes in an SL relationship with *CDH1*. In order to develop a chemopreventative drug that mutation carriers are able to take to prevent any development of cancer, and reduce the need for what is currently the only effective treatment, prophylactic gastrectomy.

1.3.1. Drug candidates for HDGC treatment

It is predicted that when *CDH1* function is lost in HDGC, druggable SL relationships emerge. A compound which targets a gene in an SL relationship with *CDH1,* would affect the viability of the *CDH1* mutant cells (cancer) allowing non-cancerous cells with healthy *CDH1* to be viable and therefore a potential new HDGC treatment to be developed [47]. Both genome-wide siRNA screening and drug screening on E-cadherin-null cell lines and their wild-type counterparts have previously been carried out in our laboratory to identify SL targets in the genome [47, 48]. The compound screen of 4,057 known drugs in a non-

malignant breast MCF10A *CDH1*$^{-/-}$ and *CDH1*$^{+/+}$ cell line, identified 21 compounds that selectively inhibited *CDH1*$^{-/-}$ cells [47]. Five drugs from two different classes were chosen to be further validated as SL compounds in this project, one statin (Atorvastatin) and four histone de-acetylase inhibitors (HDACi); Pracinostat, Entinostat, Mocetinostat and Vorinostat.

1.3.1.1. Statins

Statins are inhibitors of HMG-CoA reductase, an enzyme in the mevalonate pathway that releases cholesterol into the blood. Atorvastatin also stimulates the liver to increase uptake of more lipids, further lowering circulating blood lipid levels. Statins are widely used to lower blood cholesterol levels for cardiovascular disease[49]. Atorvastatin represents an ideal potential chemopreventative compound, as it is already prescribed to a large proportion of the population, with very minor adverse effects [49]. Atorvastatin has also previously been shown to selectively inhibit the growth of cell lines with low E-cadherin expression [50]. This is likely to be due to reducing cholesterol content in the membrane and altering the concentration of cell receptors in lipid rafts [51].

1.3.1.2. Histone De-acetylase inhibitors

There are many different classes of HDAC, most commonly found are class I, II and III. Class one is involved in death and proliferation pathways in all tissues, while class II is more tissue specific. Class III HDAC are involved in transcriptional regulation. Histone deacetylase inhibitors (HDACi) block the enzymatic removal of acetyl groups from histones. Acetylated histones are transcriptionally active, by blocking de-acetylation with HDACi these regions maintain transcriptional activity [52]. De-acetylated histones are common in cancer cells and are thought to be a potential mechanism inhibiting expression of tumour

suppressor genes such as *CDH1*, therefore blocking de-acetylation is a promising drug target [53]. HDACi's are relatively well tolerated, with the most common adverse effects being fatigue and nausea [54]. Several HDACi's are FDA approved for cancer treatment [55]. HDACi's have been shown to selectively inhibit the growth of *CDH1*$^{-/-}$ cells and therefore show promise as a potential HDGC therapeutic [47]. In this project, four HDACi were tested: Entinostat, Pracinostat, Vorinostat and Mocetinostat. As they were identified in the original high throughput screen carried out in this laboratory [47].

a) Entinostat, a benzamide HDACi that specifically inhibits class I HDAC's, which are overexpressed in some gastric cancers [56]. Entinostat is currently being assessed in phase I and II clinical trials for multiple different cancer types. Proposed mechanisms for inhibition of cancer include increased production of reactive oxygen species, apoptosis induction and cell cycle arrest [57].
b) Pracinostat is a valproic acid HDACi that targets HDACs 1,2 and 4. Clinical trials for many solid tumour forms with positive results, including stable disease for greater than 6 months. A hypothesised mechanism of action is that Pracinostat has anti-angiogenic effects within tumour tissue [58].
c) Mocetinostat is a new generation synthetic benzamide HDACi which specifically inhibits class 1 and 4 HDAC's. Phase I and II clinical trials with Mocetinostat are ongoing in a range of cancers including lymphoma, haematological and solid tumour cancers [59]. Common adverse effects include fatigue and GI toxicities, however these have not been reported as severe or unmanageable therapeutically. Adverse haematological effects have also been observed, however, these were often due to a pre-existing condition [59]. In 2014, Mocetinostat was approved by the Food and Drug Association (FDA) for the treatment of diffuse large cell B lymphoma [60].

d) Vorinostat (SAHA) is a pan-HDACi, it inhibits HDAC's 1 2 and 4 [61]. It has been FDA approved for the treatment of cutaneous T cell lymphoma (CTCL). A potential mechanism of it anti-tumorigenic effects may involve transcriptional regulation of pro-growth pathways to stop proliferation[62]. Clinical trials for all the HDACi mentioned have shown that common adverse effects are fatigue, nausea and diarrhoea, which are all effects that can be managed therapeutically.

1.4. Current models of gastric cancer

1.4.1. Cell culture model

Cell culture models of gastric cancer have been developed and characterised, and are effectively used as a first step in testing potential therapies for gastric cancer[63]. Cell culture is an important first step for the trial of any therapy as it enables for high throughput screening in environments that are easy to manipulate compared to more complex models. It also allows for clear visualisation of the cellular impact of therapies [63]. However there are issues with cancer cell lines as they are highly mutated and will evolve due to the selection pressures of cell culture. This creates cell lines that are no longer representative of the cells *in vivo* [64]. Cancer *in vivo* is also not a 2D structure, and cell culture doesn't reproduce interactions with the extracellular matrix. 2D cell modelling is a useful tool for high throughput preliminary data, where results can be further validated in a more complex 3D model.

1.4.2. Gastric organoid models

A more advanced culture model for gastric cancer is gastric organoids. As well as having a structure comparable to the gastric gland, a key feature of gastric organoids is that they contain all the cell lineages found in the stomach, not just one cell type as in 2D cell

culture[65]. They are a lower throughput model than 2D models, and still do not demonstrate the full gastric microenvironment, but are an effective intermediate step between 2D cell culture and animal models. The first gastric organoids were developed by Barker *et al*. in 2010 [65] and since then many models have been developed. This project will utilise two models, the Air-liquid interface (ALI) model and the submerged model.

1.4.2.1. Air liquid interface model

The air-liquid interface (ALI) organoid model has been previously established in the laboratory by Yasmin Nouri (MSc Candidate, Department of Biochemistry) and Tanis Godwin (ARF, Department of Biochemistry). Neonatal murine gastric tissue is embedded within a collagen matrix, and co-cultured with myofibroblasts in an inner well. This inner well sits within an outer growth medium-containing well, with medium reaching halfway up the collagen layer. This creates an air liquid interface [66].

The ALI organoid model attempts to reproduce the *in vivo* environment as closely as possible. By using the whole neonatal mouse stomach both stem cells and differentiated cells are cultured, leading to all gastric cell lineages being present in the organoids [66]. The exposure to an air-liquid interface encourages differentiation into gastric surface mucous cells. These cells are normally exposed to the lumen within an *in vivo* stomach, and are not found in other liquid only organoid models [66]. Co-culture with myofibroblasts is representative of the stromal cells *in vivo*, which release growth factors to maintain the stem cell niche[67].

1.4.2.2. Submerged model

The submerged model is generated from adult mouse stem cells (aSC's) which are obtained from the pit of the gastric glands of the pyloric end of the mouse stomach [65]. The term submerged is used as the mouse tissue is then placed within a matrix of Matrigel which is submerged in enriched growth medium [68].

The benefits of the submerged 3D organoid model is the long term culture. Organoids fully develop within a week and are then able to be passaged and cultured again. This process is able to occur for over 8 months [65]. This process is medium throughput while still providing a 3D model of gastric cancer and all the different cell lineages. It is therefore a very useful tool for the testing of novel therapeutics.

1.4.2.3. Additional models

Other organoid models include the Induced Pluripotent stem cell (iPSC) model, where iPSCs are cultured into organoids on a Matrigel coated plate. The differentiation of iPSCs into the different cell lineages is directed through the addition of specific growth factors to the culture medium. This involves the daily addition of different growth factors and inhibitors to the organoid culture to induce the differentiation into different cell types from the pluripotent stem cells. This model is therefore very labour intensive. The iPSC model is a very low throughput model as the organoids are grown for 34 days, compared to 7 days for ALI and submerged[69].

1.4.3 Mouse models

Modelling gastric cancer in mice is an important final step prior to clinical trial for any potential therapy. Mouse models of gastric cancer show the tumour in its complete microenvironment, with all cell lineages present, and other organs and body systems to

represent fully the effect of treatment *in vivo*. While not being high throughput and easily manipulated, mouse models most accurately demonstrate the effects of novel treatments before the clinical trial phase[70].

1.5. Aims

The overall aim of this project was to validate synthetic lethal compounds which selectively inhibited *CDH1*$^{-/-}$ cells, in three models of HDGC. Five compounds were studied, identified previously in our laboratory through a known drug screen. 2D and 3D models were used to identify the compound which displayed the most significant SL effect, to provide a base knowledge which can be applied to further trials for the development of a chemopreventative treatment option for HDGC patients. Ultimately, this compound has the potential to reduce both the risk of hereditary diffuse gastric cancer and the need for prophylactic gastrectomy. This aim was completed through three phases:

- Preliminary analysis of the synthetic lethal effect of five compounds, HDACi's and statins in a pair of NCI-N87 *CDH1*$^{-/-}$ and *CDH1*$^{+/+}$ isogenic gastric cancer cell lines, previously generated in the laboratory (Chen et al., 2019, manuscript in preparation).
- Analysis of the previous clinical trial data of compounds which showed a significant SL effect in the NCI-N87 cell model was done. Compounds which were already FDA approved as cancer treatments, and showed significant selective inhibition of *CDH1*$^{-/-}$ in the NCI-N87 line, were then taken to the next phase of the project: validation in the ALI organoid model.
- Thirdly a new organoid model, the submerged organoid model, was optimised to allow for a higher throughput 3D model for drug validation and to address limitations in the ALI organoid model. The submerged model was then used to further validate the SL effect of the compound with the most significant SL effect in the ALI model.

Chapter 2: Materials

2.1 List of Reagents

0.05% trypsin – prepared in the lab (dilution of 0.5% Trypsin at a 1:10 ratio with PBS)

AlamarBlue – Thermo Fisher Scientifiic, USA

Atorvastatin – Selleckchem, USA

Dimethyl sulfoxide (DMSO) – Sigma-Aldrich, USA

Dulbecco's modified Eagle's medium and F12 (DMEM-F12) – Thermo Fisher Scientific, USA

Endoxifen Hydrochloride Hydrate – Sigma-Aldrich, USA

Entinostat – Selleckchem, USA

Foetal bovine serum (FBS) – Invitrogen, USA

Freezing medium – Prepared in lab

Gentamicin (Gibco) – Thermo Fisher Scientific, USA

GlutaMAX™ Supplement – Thermo Fisher Scientific, USA

Hoechst 33342 - Thermo Fisher Scientific, USA

Mocetinostat – Selleckchem, USA

Nitta cellMatrix Collagen Gel Culturing Kit – Novachem, Australia

Paraformaldehyde (PFA) – BDH Limited, England

Phosphate buffered saline (PBS) solution – Prepared in lab

(1 PBS tablet dissolved in 100 mL H_2O, then autoclaved to sterilise.)

Pracinostat – Selleckchem, USA

Saponin – Sigma-Adrich, USA

Vorinostat (SAHA) – Selleckchem, USA

2.2 List of Equipment

1 mL cryovials – Nunc, Denmark

1.5 mL Eppendorf tubes – Sigma-Aldrich, USA

10 mL serological pipettes – Greiner Bio-One, Germany

10 cm Cellstar cell culture dish – Greiner, Germany

15 mL Falcon tubes – BD Biosciences, USA

24 well clear, flat bottom plates- Corning, USA

30 mm Cellstar cell culture dish – Greiner, Germany

50 mL Falcon tubes – BD Biosciences, USA 500 mL filter system - Corning, USA

60 mm Cellstar cell culture dish – Greiner Bio-One, Germany

75 mL cell culture flasks – Greiner Bio-One, Germany

96 well black walled, clear, flat bottom plates – Corning, USA

Centra 3C centrifuge – International Equipment Company, USA

CO_2 cell culture incubator – Binder, Germany

ClarioSTAR microplate reader – BMG labtech, Germany

Cytation 5 Imaging reader – BioTek, USA

Dual chamber cell counting slides – Bio-Rad, USA

Luna-II™ Automated cell counter – Logos Biosystems, South Korea

Millicell cell culture inserts (0.4µm, 30mm) – Merck Millipore, Ireland

Mr. Frosty 5100 Cryo 1°C Freezing Container – Thermo Fisher Scientific, USA

Olympus CK2 Microscope – Olympus, New Zealand

Tissue culture hood – EMAIL, Australia

Water bath – Semco, USA

2.3 Software

ImageJ – National Institute of Health, USA

GraphPad Prism version 7.00 for Windows, GraphPad Software - La Jolla California USA

Gen-5 software – Biotek, USA

R version 3.6.0 - R Foundation for Statistical Computing, Vienna, Austria. [81]

2.4 Ethics

All animal procedures were completed according to University of Otago guidelines and regulations and approved by the University of Otago Animal Welfare and Ethics Committee.

Chapter 3: Methods

3.1. NCI-N87 culture

NCI-N87 cells are a human gastric cancer epithelial cell line obtained from a high grade liver metastasis, therefore these cells have a high level of background mutations representative of *in vivo* cancerous tissue. An isogenic pair of NCI-N87 *CDH1*$^{+/+}$ and *CDH1*$^{-/-}$ cell lines were generated previously by the Cancer Genetics laboratory through CRISPR-Cas9 methodology (Chen et al., 2019, manuscript in preparation).

NCI-N87 cells are an adherent culture. Cells were grown in 75 mL angled neck cell culture flasks at 37°C and 5% CO2 in a humidified incubator. Complete culture medium contained 80% Dulbecco's modified Eagle's medium and F12 (DMEM-F12) and 20% filtered (0.22 µm filter) foetal bovine serum (FBS). NCI-N87 cells were passaged once 80-90% confluence was reached. Prior to passage, 0.05% Trypsin-EDTA, PBS and complete growth medium were pre-warmed at 37°C in a water bath. Medium was aspirated from the flask and cells were washed with 5 mL PBS to remove any remaining growth medium. Then 3 mL of 0.05% trypsin-EDTA was added to the flask and left to incubate at 37°C for 5 minutes. 6 mL of complete growth medium was then added to each flask to neutralise trypsin activity and the cell suspension transferred to a 15 mL falcon tube. Cells were then centrifuged at 100 RCF for five minutes. Supernatant was aspirated and the pellet resuspended in 1 mL of complete growth medium.

Cells were counted using a Luna-II™ Automated cell counter and re-seeded. 10 µL of resuspended cells was added to each end of a dual chamber counting slide. Two measurements of cell concentration were averaged, then used to calculate density of resuspended cells. NCI-N87 *CDH1*$^{+/+}$ and *CDH1*$^{-/-}$ cells were plated at respective densities of

$1x10^6$ and $1.1x10^6$ cells per 75 mL cell culture flask. This seeding density allows both cell types to reach 80-90% confluency within seven days. Growth medium was changed every 3 days during culture.

3.1.1. Resurrection of NCI-N87 cells

NCI-N87 cells were stored in liquid nitrogen vapour phase for long term storage. Cells were removed from liquid nitrogen and thawed in a 37 °C water bath. Cells were resuspended in 9 mL of complete growth medium to dilute any remaining DMSO from the freezing medium, as DMSO is toxic to cells at temperatures above room temperature. Cells were then centrifuged at 100 RCF for 5 minutes. Supernatant was aspirated and the cell pellet resuspended in pre-warmed complete growth medium. Resuspended cells were then seeded into 75 mL cell culture flasks and incubated at 37°C and 5% CO_2 in a humidified incubator. Growth medium was changed the following day to remove any non-adherent dead cells.

3.1.2. Cryogenic preservation of NCI-N87 cells

Following the passage protocol in methods section 3.1, after trypsinisation, cell pellets were resuspended in freezing medium (80% complete media, 10% FBS and 10% DMSO) instead of complete growth medium, and aliquoted into 1 mL cryovials. Vials were then placed into a Mr Frosty Cryo 1°C Freezing Container transferred to the -80°C freezer for 24 hours. This froze cells at a rate of 1°C per minute. After 24 hours, vials were removed from the -80°C freezer and placed into liquid nitrogen for long term storage.

3.1.3. NCI-N87 drug screening

Drug aliquots were reconstituted in DMSO and stored at -20°C. Individual drug aliquots were further diluted in complete growth medium to create working stocks on the day of the assay.

Cells were seeded in a 96-well plate (black walled, clear bottomed) at 10,000 cells per well in 90 µL of complete growth medium. Plates were then incubated at 37°C and 5% CO_2 in a humidified incubator. After 24 hours of incubation cells were treated with 10 µL drug or 10 µL of 0.1% DMSO for negative control wells. The concentration of DMSO used was below the previously identified toxic concentration of 0.2%. A serial dilution of each drug was performed with concentrations ranging from 0.31 µM to 40 µM. Three technical replicates were done per experiment. The experiment was repeated in triplicate and the results averaged.

WT										
CDH1$^{+/+}$	DMSO	40µM	20µM	10µM	5µM	2.5µM	1.25µM	0.63µM	0.31µM	DMSO
	DMSO	40µM	20µM	10µM	5µM	2.5µM	1.25µM	0.63µM	0.31µM	DMSO
	DMSO	40µM	20µM	10µM	5µM	2.5µM	1.25µM	0.63µM	0.31µM	DMSO
KO	DMSO	40µM	20µM	10µM	5µM	2.5µM	1.25µM	0.63µM	0.31µM	DMSO
CDH1$^{-/-}$	DMSO	40µM	20µM	10µM	5µM	2.5µM	1.25µM	0.63µM	0.31µM	DMSO
	DMSO	40µM	20µM	10µM	5µM	2.5µM	1.25µM	0.63µM	0.31µM	DMSO

Figure 4: 96 well plate plan for NCI-N87 drug assay.
Green = 10,000 NCI-N87 CDH1$^{+/+}$ or WT cells per well. Grey= 10,000 NCI-N87 CDH1$^{-/-}$ or KO cells per well. Each cell type was treated with a serial dilution of drug, in triplicate for each concentration. Outer wells were used for a 24 hour edge count to validate seeding accuracy.

3.1.3.1. 24 hour edge count

24 hours after seeding cells, a seeding accuracy check was completed. Cells in the outer wells were stained with Hoechst (1 µg/mL) in PBS and the plate was read in the cytation 5 imaging reader at 37°C and 5% CO_2. Six images were taken per well at 4x objective, with excitation and emission wavelengths of 377 and 447 respectively (Figure 4). The Gen5 software analysed fluorescence intensity and performed segmentation of nuclei to determine a total nuclei count per well.

3.1.3.2. Cell viability assay

After 48 hours of drug treatment, a total nuclei count was performed. Cells were fixed and stained with 0.075% saponin, 1 µg/mL Hoechst, and 0.25% paraformaldehyde solution (PFA) in PBS. Due to fixation, saponin was used as Hoechst is not able to penetrate the membrane of dead/fixed cells. 100 µL of this solution was added to each well of the 96-well plate on top of the media. Plates were left at room temperature in the dark for 30 minutes to allow the light sensitive solution to stain the nuclei. Plates were imaged in the cytation 5 imaging reader at 6 fields per well. The Gen5 software calculated total nuclei counts from these images.

3.1.3.3. Statistical analysis

Prism software was used for the statistical analysis of NCI-N87 drug data. Drug concentration data was averaged and normalised to the respective *CDH1*$^{+/+}$ and *CDH*$^{-/-}$ DMSO controls, to account for any potential impact of the DMSO vehicle on cell viability. Grouped analyses with multiple un-paired student's t-tests were performed for each drug, assuming non-consistent standard deviation. Statistical significance was determined as an adjusted p-value less than 0.05, correcting for multiple comparisons using the Holm-Sidak method.

3.2. Air-liquid interface Organoid model

3.2.1. Myofibroblast culture

Myofibroblasts are a cell type found in mucosal surfaces like those of the gastrointestinal tract. When cultured they are an adherent cell type which look phenotypically similar to a fibroblast or smooth muscle cells [71]. The role of the myofibroblast in the mucosa is

structural and also involved in immune homeostasis, hence they are an important co-culture for the growth of gastric organoids [71].

The Myofibroblasts cell line (MFB11) used in the ALI organoid protocol were previously isolated in the laboratory from a wildtype C57 Black 6 mouse (C57BL/6) using a protocol adapted from Pastula *et al.* [72]. MFB11 were used between passage 15 to no later than passage 22 for co-culture with organoids. MFB11 cells were cultured in a humidified incubator at 37°C with 5% CO_2 in 75 mL cell culture flasks. MFB11 complete culture media was made using Gibco DMEM/F-12 GlutaMAX™ supplement (80%) and 20% filtered FBS (0.22 µm filter).

3.2.1.1 Passage

The protocol for passage of the MFB11 cells is as per the passage protocol for the NCI-N87 cells, as described in methods section 3.1. Minor changes to the protocol include incubation in 0.05% trypsin for 8 minutes and resuspension of cells in MFB11 media. Cells were then counted using the LUNA automated cell counter and re-seeded at $1x10^5$ cells per 75 mL cell culture flask. At this seeding density MFB11 reached confluency in seven days. Complete culture media was changed every three days and cells passaged every seven days.

3.2.1.2 MFB11 Resurrection

Resurrection of MFB11 cells is as per the protocol for NCI-N87 cells, described in methods section 3.1.2.

3.2.1.3. Cryogenic preservation

Cryopreservation of MFB11 cells is as per the cryopreservation protocol for NCI-N87 cells, described in methods section 3.1.3.

3.2.2. Air-Liquid Interface Organoid Drug assay preparation

The protocol used for the drug assay using the Air-liquid interface (ALI) organoid model has been developed and optimised in the laboratory by Yasmin Nouri and Tom Brew (PhD candidate, Department of Biochemistry).

3.2.2.1. MFB co-culture preparation

Six wells of ALI organoids were cultured for each drug assay, requiring a total of 6 x 10^6 MFB11 cells for co-culture. Therefore, for every drug assay approximately thirteen confluent 75 mL flasks of MFB11were required. MFB11 passage was completed initially as per protocol described above (Methods section 3.2.1.1.). After centrifugation, MFB11 were instead resuspended in 10xF12 Growth medium and cells pooled together in a 15 mL falcon tube.

A dilution of 1:5 was done to allow for accurate cell counting, 10µL of this dilution was added to a dual chamber counting slide and cell count obtained. Two measurements of cell concentration were done, these were averaged to determine the density of resuspended cells. MFB11 were then placed on ice for organoid preparation.

3.2.2.2 Organoid culture

3.2.2.2.1. Collagen preparation: *Base Layer*

A Collagen matrix was used for the growth of ALI gastric organoids. Work done with collagen was always on ice, as collagen sets at room temperature. For an ALI organoid

drugging protocol, six 30 mm dishes of organoids were required. 2.4 mL of collagen was used per well with an extra 30% to account for collagen wastage. Therefore, a total of 9.36 mL collagen mix was prepared for the base layer, containing only MFB11.

This included: 7.488 mL collagen, added to the tube on ice first so other components could be easily dispersed throughout the viscous solution. A 0.936 mL solution containing $3.9x10^6$ MFB11 cells in F-12 Growth media. Lastly 0.936 mL of sodium bicarbonate, this was then gently mixed using a 10 mL stripette.

Six 30 mm Milicell raised transwell inserts were placed inside 60 mm cell culture dishes. 1.2 mL of the complete collagen solution was added to each of the six transwell inserts, lids were placed on the outer (60mm) dish and placed in the incubator at 37°C for 30 minutes for the collagen to set. The 15 mL falcon tube containing residual collagen with MFB11 in media and sodium bicarbonate was placed on ice and re-used for the preparation of the second layer, to avoid collagen wastage.

Table 1: Concentration of components in CellMatrix™ collagen gel culturing kit for culture of the ALI organoid model

Reagent	Concentration (%)
cellMatrixTM collagen solution Type I-A	80
10x Ham's F-12 growth medium	10
Sodium bicarbonate buffer solution	10

3.2.2.2.2 Mouse Euthanasia and stomach extraction

Organoids were generated from 24-48 hour old mouse pup gastric stem cells. These mice were inducible knockout mice that have a cre-lox system controlling the knockout of *CDH1*$^{-/-}$ and the fluorescent marker Tdtomato under the CD44 promoter (*CD44*-cre/*Cdh1*-/-

/TdTomato). Mice were Euthanised by through decapitation by a sterile single-edge 10cm razor blade in a sterile 100mm dish. A sterile lid was placed over the dish and the mouse was then transferred to the tissue culture hood for stomach extraction.

3.2.2.2.2.1 Stomach Extraction

Once within the tissue culture hood, the mouse body was transferred from the dish in to the clean lid for stomach extraction. External specific scissors and forceps were used to complete the extraction. First forceps were used to manoeuvre the front and hind legs apart so that the stomach could be seen. Stomach was identifiable through the transparent skin of the mouse pup, as a large white organ under the skin on the right hand side. Sterile external specific scissors are used to cut directly above the stomach, which was then able to be pulled out through the incision by the forceps. Scissors were used to remove any additional gastrointestinal tissue that was attached to the stomach. The stomach was then placed in a 30mm dish on ice containing 1mL of PBS with 50 µg/mL gentamicin for the first wash step.

3.2.2.2.2.2 Stomach tissue wash

External forceps and scissors were placed in ethanol to sterilise for the remaining stomach extractions. Sterile internal forceps and scissors were used for the four washes of the stomach. The stomach was gently cut open and all residual milk removed, this was done through gently pressing the forceps along the stomach so the milk residue is pushed out of the incision. Stomach tissue was transferred from each dish containing 1mL PBS and 50 µg/mL gentamicin to the next, four times, until the stomach was clean and all milk had been expelled. The whole stomach was then transferred to a 1.5 mL Eppendorf containing 100 µL PBS and 50 µg/mL gentamicin. Internal forceps and scissors were placed in ethanol to sterilise, while the second mouse was euthanised and brought into the tissue culture hood. This process was repeated four times for each ALI drug assay. All four stomachs were placed

into the same 1.5 mL Eppendorf with 100 µL PBS and gentamicin. For each new stomach extraction, sterile forceps and scissors were used, and 1mL PBS and gentamicin 50µg/mL was refreshed in each wash well.

Once all four stomachs were in the 1.5 mL Eppendorf in 100 µL PBS and gentamicin, scissors were used to roughly mince the stomach tissue. Once the stomach tissue was as fine as possible, the smaller <0.5mm^3, Westcott tenotomy scissors were used to even further mince the tissue ready for seeding.

3.2.2.2.3 Collagen preparation: *Tissue layer*

Once the stomach tissue was minced the second layer of collagen solution was prepared, using to the same ratio as for the first layer. A total of 9.36 mL was required for the 6 wells; 7.448 mL collagen, 0.936 mL MFB in F12 growth media and 0.936 mL Sodium bicarbonate were combined in the 15 mL falcon tube used for the first collagen layer preparation (Table 1). Minced stomach tissue within 100 µL of PBS and gentamicin, was spun at 800 g for 2 minutes so that tissue collected at the base of the Eppendorf tube. The supernatant was aspirated, and tissue fragments were resuspended in 1 mL of the second layer collagen mix. This 1 mL of collagen containing stomach fragments was then transferred back to the 15 mL falcon tube containing the rest of the collagen mix, and gently and evenly mixed throughout. Inserts containing the now-set first layer of collagen, were removed from the incubator and placed inside the tissue culture hood. 1.2 mL of the 2nd layer collagen mix containing stomach tissue was added to each well. This was done carefully as to evenly distribute the stomach tissue around the well, so that organoids grew spread over the insert not all in the middle. Inserts containing a complete 2.4 mL of collagen were then placed back into the incubator at 37°C to set for 30 minutes.

3.2.2.2.4 Induction of *CDH1* knockout

Complete growth media for ALI organoids was made up of 80% F-12 GlutaMAX™ supplement media, with 20% FBS and 0.1% Gentamicin. To induce knockout (KO) of *CDH1* and activation of TdTomato, endoxifen was added at a concentration of 5 µM to the media on day 0. Endoxifen is a metabolite of tamoxifen, which induces cre-lox activation. For the day 0 wild type *CDH1* media, the equivalent amount of DMSO was added, as this was the vehicle for endoxifen. Identification of TdTomato fluorescence through microscopy in organoids treated with endoxifen, was used to confirm *CDH1* knockout. It has been previously validated in our laboratory that organoids expressing TdTomato have approximately 73% homozygous knockout of *CDH1 [73]*.

Once collagen was set, 3 mL of complete growth media containing either endoxifen or DMSO, was added to each of the outer 60mm dishes (Figure 5). Three dishes of each condition, WT and KO were generated in preparation for the drug assay. Organoids were then placed in an incubator (37 °C, 5% CO_2) for two days until drug treatment was added.

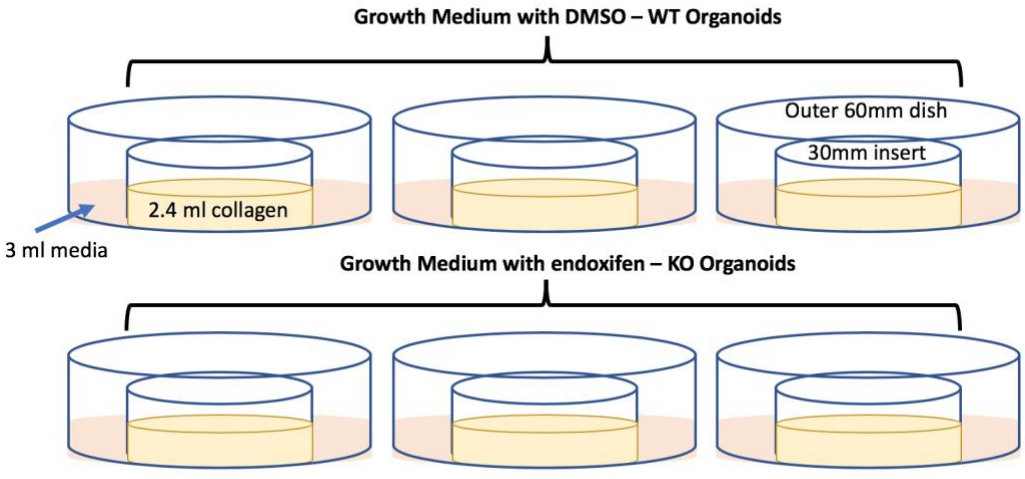

Figure 5: Diagram of ALI organoid drug assay preparation.
Organoids sit within a 2.4 mL collagen layer, in a 30mm insert. This sits within a larger 60mm insert, containing 3 mL of complete growth medium. Top: Three CDH1 WT wells, treated with DMSO. Bottom: Three CDH1 KO wells, treated with Endoxifen.

3.2.3. ALI drug screening

After two days of culture at 37 °C and 5% CO_2 in the incubator organoids were treated with drug. Media was removed from the outer well and replaced with 3 mL of media containing the drug at the required concentration. This treatment concentration was determined from the preliminary NCI-N87 cell culture drug screen data. Each treatment condition was added to two wells, one WT and one KO (Figure 6). A single WT/KO DMSO treated control was used for both drugs as the conditions of the experiment were the same. DMSO toxicity is seen in ALI organoids at concentrations higher than 0.05%, so for all experiments the final concentration of DMSO was 0.02%. Organoids were placed back into the incubator at 37 °C, 5% CO2, and treated with drug for four days, until day 6 of the assay.

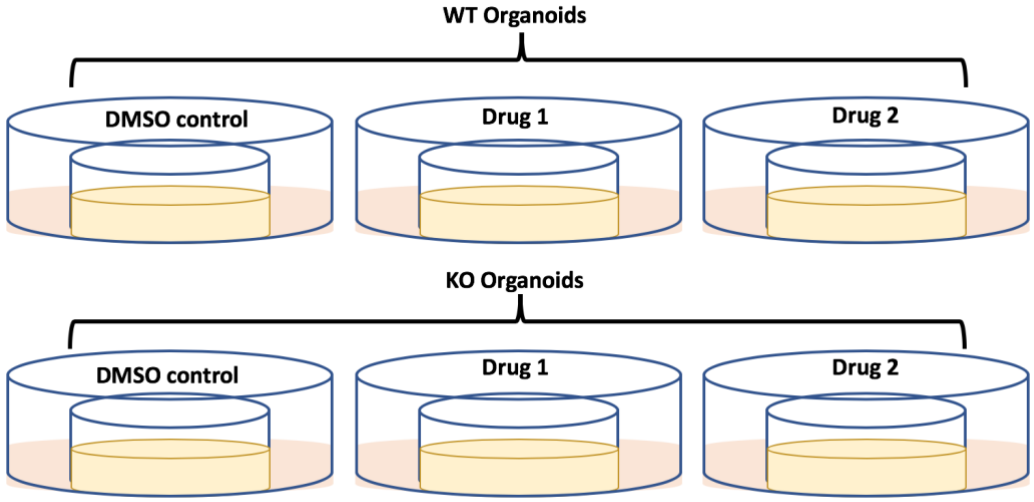

Figure 6: Diagram of well conditions for ALI organoid drug assay.
Three wells for both CDH1KO and CDH1 WT organoids, each WT and KO pair was to be treated with a different condition: DMSO, Drug 1 or Drug 2.

3.2.3.1.Quantification of ALI organoid viability

Organoids were imaged daily through brightfield microscopy on the Eclipse Ti Inverted microscope using the Fuji LAS-3000 ECL Imaging system, to track organoid growth. On day 2 when drug treatment first started, and day 6, the final day of the assay, fluorescent images

were also taken. This was done on the Inverted microscope through the TRITC filter, to identify TdTomato fluorescence and successful *CDH1* knockout. When imaging the organoids, the transwell insert remained within the outer 60mm dish.

Brightfield images taken on day 2 (Day 0 of drug treatment) and day 6 (Day 4 of drug treatment) were used to quantify impact of the drug on organoid viability, through measuring change in organoid area. Using the measure tool on FIJI (ImageJ) the outline of each organoid was traced and an area measurement calculated. These two measurements allowed a growth change to be calculated for each individual organoid, and analysis of impact on growth from treatment to be completed.

3.2.3.2. Statistical analysis

Statistical analysis was undertaken in consultation with Associate Professor Mik Black (Department of Biochemistry, University of Otago). Area data of organoids on day 2 and day 6 obtained from FIJI were logged (natural log), and the log-difference in area (day 6 minus day 2) was calculated for each sample. A single outlier observation (25-fold area increase over 4 days) was removed due to this being an implausible growth rate, most likely resulting from an error in the initial area estimate.

Standard deviations were calculated per technical replicate, and these were used to determine the variability associated with each estimated log difference in area (average per technical replicate). For both KO and WT, each drug (Vorinostat and Mocetinostat) was standardised to DMSO by subtracting the mean (log scale).

A standardised estimate for the log difference in area was then calculated, and standard error calculated by combining error estimates from both technical and biological replicates, this is equivalent to using non-pooled standard deviation. Data were anti-logged to present as a percentage scale relative to DMSO. The mean difference in area estimates are presented as bar charts with associated standard error bars. These mathematical transformations were completed to take into consideration both technical and biological replicates and variability in the data.

3.2.4 ALI-halo Organoid Analysis

ALI organoids were seen to develop into two distinct phenotypes, true organoids and 'halo' organoids. The ALI drug assay was complete after 6 days, when the final area measurement was completed. However on day 6 the halo organoids appeared to disintegrate in the *CDH1*$^{-/-}$ wells treated with drug. To understand this interesting artefact and see if there was an SL effect occurring in these structures, halo organoids were imaged for a further 6 days, until day 12 to see the impact of the drug over a longer term assay. Media was changed every three days however no further drug was added. A blinded assay on halo integrity was then carried out to investigate whether a SL effect could be seen in these structures. Halo organoid images from day 12 were blinded and then analysed for halo integrity. Analysis was done by at least two fully blinded individuals. If an image had a variation in integrity score it was further analysed by two other individuals. This assay was only completed once due to time constraints.

3.3. Submerged Organoid model

The protocol for the culture of submerged organoids was adapted from the established protocol developed in the Clevers laboratory ([65, 68].

3.3.1. Organoid preparation from primary tissue

3.3.1.1. Stomach extraction

For the preparation of inducible *CDH1* knockout submerged organoids, *CD44*-cre/*Cdh1*-/-/TdTomato mice were used, at between six to eight weeks old.

Mice were euthanised through CO_2 administration. Once breathing had ceased a cervical dislocation was done for confirmation of death. Stomach extraction was then completed. To do this, the mouse was placed onto a flat surface and pinned outstretched so that the abdomen was facing upward. Mouse abdomen was wet with 70% ethanol prior to the stomach removal procedure. A mucosal layer incision was done from the external genitalia to just below the rib cage. Skin was then pinned back to allow for a second incision into the mucosal layer, removing the abdominal musculature from the abdominal cavity. The stomach is situated on the right hand side, behind the liver and black in appearance. New sterile forceps and scissors were then used to remove the stomach from the abdominal cavity and remove any other gastro-intestinal tissue (oesophagus and duodenum). The whole stomach was then placed into a 50 mL falcon tube containing ice cold PBS.

3.3.1.2. Gastric gland isolation and seeding

Stomach was removed from 50 mL falcon and placed in a 10 cm dish. Stomach was opened along the greater curvature, which spans from the oesophagus to the duodenum. To remove mucus, the open stomach was washed twice in two 10 cm dishes each containing 35 mL of PBS. Once washed, dissection of the antral stomach was done, the antrum is pale in comparison to the body of the stomach.

The antral stomach was placed in a 50 mL falcon containing 25 mM EDTA, a chelating buffer and placed on a roller for 90 minutes at 4 ºC, this was done to loosen the adhesion between glands and the underlying stroma. Stomach was then removed from chelating buffer and placed into a 50 mL falcon tube containing 10 mL of ice cold PBS. This tube was shaken ten times to release the gastric glands from the stromal tissue into the PBS. Sterile forceps were used to remove any large pieces of tissue from the solution. This was then spun for 5 minutes at 200 g at 4 degrees. Supernatant containing PBS was removed and the glands were resuspended in 10 mL of ice cold basal medium.

To isolate the glands from the solution, the suspension was passed through a 70µM cell strainer into a 15 mL falcon tube on ice. Extra basal media was washed through the strainer to obtain all the gastric glands, large pieces of muscle tissue not required for the organoid prep cannot pass through the strainer. The basal medium containing gastric glands was then spun at 200 g for five minutes at 4 degrees, then supernatant was removed leaving only gland tissue in the tube. Maximum amount of supernatant was removed as Matrigel proteins can be diluted inhibiting organoid growth. The glands were resuspended in the quantity of Matrigel required for seeding (50 µL per well) plus 10% extra to account for the dead volume of Matrigel. 50 µL of this Matrigel/gastric gland suspension was placed into each well required of a pre-warmed 24 well plate. Plate was then placed in the incubator at 37°C for 10 minutes to allow Matrigel to set. 500 µL of complete submerged growth medium was added to each well (Table 2) and the plate placed back into the incubator at 37°C and 5% CO_2. The initial organoid preparation from the mouse gastric tissue was done in our lab by Tom Brew.

3.3.2. Media components

Complete growth medium was prepared fresh for each medium change according to the concentrations in Table 2. Once all components of the medium were combined, media was

placed in the water bath to warm to 37°C prior to addition to organoids. Basal medium was prepared according to Table 3, as needed and stored at 4°C. When required for use, basal media was placed on ice.

Table 2: Complete growth medium for submerged organoids

Reagent	Final concentration
Advanced DMEM/F12	N/A
HEPES	10 mM
GlutaMAX	2 mM
Pen/Strep	1x
N-acetylcysteine	1 mM
Gastrin	10 nM
EGF	50 ng/mL
R-Spondin1-conditioned medium	10%
Noggin-conditioned medium	10%
FGF10	100 ng/mL
Wnt3a-conditioned medium	50%
Y-27632 (RHOK inhibitor)	10 µM
B27	1x
N2	1x
A 83-01	2 µM

Table 3: Basal medium for submerged organoid passage

Reagent	Final concentration
Advanced DMEM/F12	N/A
HEPES	10 mM
GlutaMAX	2 mM
Pen/Strep	1x

3.3.3. Submerged organoid culture

Submerged organoids were grown at 37°C, 5% CO_2 in an incubator, within a 24 well plate in 500 µL media. Media was made as per table 2, and was changed every 3 days.

3.3.3.1. Submerged organoid passage

After 7 days of growth, submerged organoids were passaged. 500 µL media was aspirated from each well so that 50 µL Matrigel dome was exposed. 1 mL cold basal medium (Table 3) was added to the well and vigorously pipetted up and down to disrupt the Matrigel. A 1mL pipette tip was also used to physically scrape Matrigel in the well. This organoid and Matrigel suspension in basal media was then transferred to a 15 mL falcon tube. Up to three wells were pooled together in this process, as increased quantities of Matrigel lead to difficulties in organoid isolation. Cold basal media was added to the falcon tube until the solution reached 15 mL. This organoid suspension was then centrifuged at 4°C for 5 minutes at 200 g. Supernatant (basal media and Matrigel) was removed, leaving 2 mL at the base of the falcon tube. The organoid pellet was then resuspended in this 2 mL solution. Organoids were then further mechanically disrupted with a 20 G needle attached to a syringe, by aspirating and dispensing the entire solution six times. Cold basal media was added so the solution was again 15 mL. The solution was then centrifuged at 100 RCF for 5 minutes at 4°C. All supernatant was aspirated from the organoid fragment pellet. Fragments were resuspended in 150 µL Matrigel using precooled pipette tips and counted on a haemocytometer.

Organoid fragments were re-seeded at 500 fragments in 50 µL of Matrigel per well. Matrigel containing organoid fragments was gently pipetted using pre-cooled pipette tips, to the centre of each well in the pre-warmed 24 well plate. Pipette tips were pre-cooled to stop Matrigel polymerisation and wastage during seeding, and the 24 well plate pre-warmed so Matrigel polymerised quickly once in the well, creating a defined Matrigel dome. Plate was placed back into incubator for 10 minutes to allow Matrigel to fully polymerise. 500 µL of complete submerged organoid growth media (Table 2) was then added to each well. PBS was added to

remaining empty wells to reduce evaporation effect. Media was changed every three days and organoids cultured for 7 days until the next passage was required.

3.3.4. Submerged organoid drug screening

For the drug screening protocol, submerged organoids were grown from single cells rather than fragments, to allow for uniform organoid growth. Methods section 3.4.3.1. Submerged organoid passage was adapted for organoid single cell preparation. Following on from the six aspirate – dispense cycles with the 20 G needle, the organoid suspension was further fragmented using a 1 mL pipette. Organoid suspensions were then pooled if more than 3 wells were passaged. Basal medium was added to the organoid fragment suspension to a volume of 15 mL. The suspension was then centrifuged at 200 RCF at 4°C for five minutes.

Supernatant was aspirated and organoid fragments resuspended in 1 mL of 0.05% Trypsin-EDTA, which was pre-warmed to 37°C. Fragment suspension in trypsin was then placed into the incubator and left for 10 minutes to generate single cells. Every two minutes 10 µL of the suspension was placed in a cell counting slide and percentage of single cells was checked to ensure over digestion did not occur. After 10 minutes 10 mL of medium containing 20% FBS was added to the suspension to quench trypsin activity. The suspension was then centrifuged for 5 minutes at 500 RCF at 4°C to pellet. Supernatant was discarded and organoid single cells were resuspended in Matrigel and counted on the LUNA automatic cell counter.

1000 organoid single cells were added in 50 µL of Matrigel to each well of a pre-warmed 96 well black walled, clear flat bottom plate. Three wells were seeded with Matrigel containing no organoid cells as a blank for the viability assay to read background fluorescence. Matrigel was added with pre-cooled pipette tips, slowly pipetting upward in the centre of the well.

This was done to avoid the spread of organoids to the edge of the well. Plated organoids were then placed back in the incubator at 37 °C for 10 minutes for the Matrigel to polymerise. 100 µL of complete growth media was then added to each well.

3.3.4.1. CDH1 knockout Induction

To induce knockout of *CDH1* and activation of TdTomato, endoxifen is added at a final concentration of 5µM to the media after 24 hours. Endoxifen is a metabolite of tamoxifen, which induces cre-lox activation. The Endoxifen is added in 100 µL of complete growth medium, which is added on top of the original 100 µL of medium in the well, so organoids are not disrupted. For the day 1 wild type $CDH1^{+/+}$ media, the equivalent amount of DMSO is added, as this is the vehicle for endoxifen.

3.3.4.2. Drug addition

On day two, a serial dilution of drug was produced with each dilution being double the concentration required in the assay. 100 µL was aspirated from each well in the plate, and 100 µL of drug in complete growth medium was added. As 100 µL of complete growth media was still present in the well, the drug concentration was doubled. Plate was placed back into the incubator and cultured until viability was assayed after 48 hours.

3.3.4.3. Viability assay

The AlamarBlue metabolic assay was utilised to analyse submerged organoid metabolic activity, which was used to infer organoid viability. This is a fluorescent assay where metabolically active cells are able to convert a non-fluorescent blue reagent Resazurin to a fluorescent product resorufin. While non-viable cells are not able to convert Resazurin to the fluorescent product. Submerged organoids were incubated in complete growth medium

supplemented with 10% AlamarBlue, for 18 hours at 37 ºC and 5% CO_2. This analysis was done after 48 hours of drug treatment. Total fluorescence was analysed on the CLARIOstar microplate reader.

3.3.5. Cryogenic preservation

Freezing media was prepared as per Table 4, and pre-cooled. Protocol for passage of submerged organoids was followed, however instead of re-suspension in Matrigel, fragments were resuspended in Advanced DMEM/F12 and counted. Submerged organoids were frozen at 1000 fragments per cryo-vial. The quantity of submerged organoids was added to each vial, and then topped up to 1 mL total solution with Freezing media, as per Table 4. Cryo-vials were placed into a Mr Frosty and quickly placed into the -80°C freezer overnight. DMSO is toxic to cells at room temperature, hence why freezing media is pre-cooled and why the Mr frosty is swiftly placed at -80°C. Cryovials are then transferred to liquid nitrogen for long term storage.

Table 4: Submerged organoid freezing medium

Reagent	Concentration
Advanced DMEM/F12	80%
Fetal Bovine Serum (FBS)	10%
DMSO	10%

3.3.6. Resurrection of submerged organoids

Cryo-vials of frozen submerged organoid fragments were removed from LN_2 and defrosted in a 37 °C water bath. After defrosting, fragments were immediately transferred to 15 mL Falcon tubes containing 5 mL of basal media (Table 3) and centrifuged at 200 g at 4°C for 5 minutes to pellet. Supernatant was then removed and fragments were resuspended in Matrigel. Matrigel containing organoid fragments was then seeded in 24 well plates – one

vial into one well- and left to polymerise for 10 minutes. Then 500 µL of complete culture media was added to each well. Culture protocol is then followed as described in section 3.3.3.

Chapter 4: Results

4.1 NCI-N87 drug assay data

The initial phase of this project involved validating the SL effect of compounds identified in the known drug screen (see section 1.3.1.) through testing in the gastric cancer NCI-N87 *CDH1*$^{+/+}$ and *CDH1*$^{-/-}$ isogenic cell lines. This 2D model allows for high throughput screening of potential SL candidates at multiple concentrations and validation of effectiveness in a gastric cancer cell line. The NCI-N87 drug assay was carried out according to the protocol described in methods section 3.2. Drug effect was analysed through a measurement of nuclei count, which was used to infer cell viability.

4.1.1. Atorvastatin

To test the SL effect of Atorvastatin, NCI-N87 cells were treated with a concentration range from 0.31 µM to 40 µM according to the protocol described in the methods section 3.2. None of the tested concentrations show a significant SL effect, with *CDH1*$^{-/-}$ cells maintaining a similar nuclei count compared to *CDH1*$^{+/+}$ cells, particularly at lower drug concentrations (Figure 7). At concentrations above 5 µM, although not statistically significant, there is a suggestive SL trend with lower *CDH1*$^{-/-}$ cell nuclei count compared to *CDH1*$^{+/+}$ (Figure 7). The closest concentration to a significant SL effect is the 20 µM concentration with an adjusted p-value of 0.069.

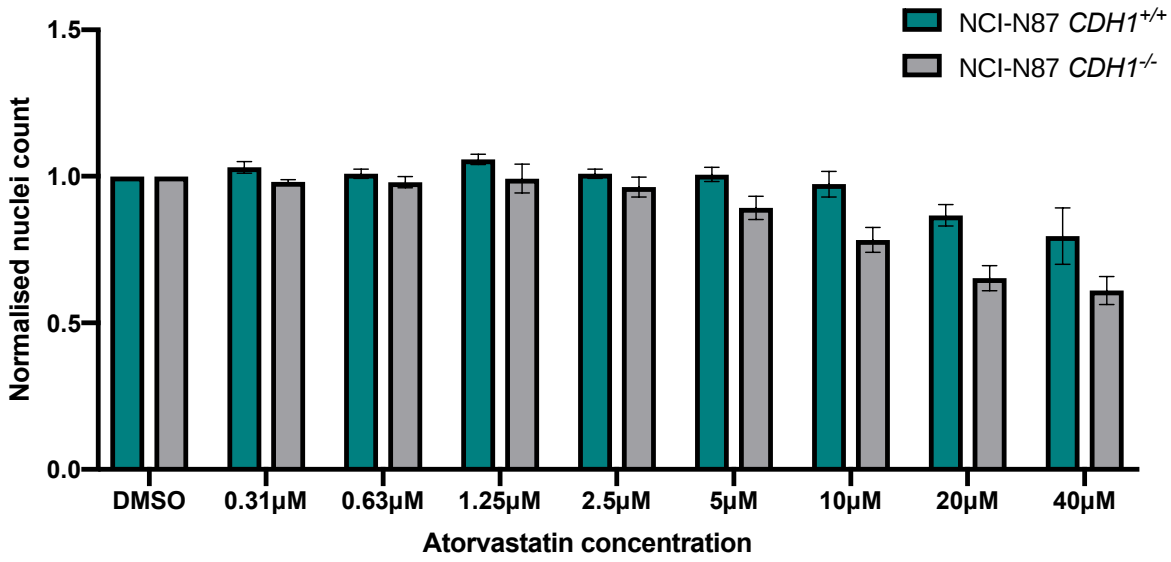

Figure 7: Normalised nuclei counts 48 hours post treatment with a serial dilution of Atorvastatin.
An isogenic pair of NCI-N87 cells used: CDH1$^{+/+}$ (green bars) and CDH1$^{-/-}$ (grey bars). Cells were treated with a serial dilution of Atorvastatin, ranging from 0.31 µM - 40 µM. No significant difference between NCI-N87 CDH1$^{+/+}$ and NCI-N87 CDH1$^{-/-}$ cell viability was observed. Data represents averaged values of four biological replicates with standard error shown. Holm-Sidak adjusted p-values were calculated using student's t-test.

4.1.2 Histone Deacetylase inhibitors

The four histone deacetylase inhibitor (HDACi) compounds identified as SL in the preliminary known drug screen [47] were validated in the NCI-N87 *CDH1*$^{-/-}$ and *CDH1*$^{+/+}$ model. Cells were treated with a range of concentrations of four HDACi: Entinostat, Pracinostat, Mocetinostat and Vorinostat. Cells were treated for 48 hours and viability analysed through a Hoechst stain nuclei count on the Cytation plate reader according to the protocol in methods section 3.2. All four HDACi tested showed a significant SL effect at one or more concentrations.

4.1.2.1 Entinostat

Entinostat specifically inhibits class I HDACs, which are known to be overexpressed in some gastric cancers [56]. Entinostat showed a significant SL effect at concentrations of 1.25 µM,

2.5 µM and 40 µM. Adjusted p-values were 0.029, 0.011 and 0.049, respectively. All other concentrations show an SL trend, with *CDH1*$^{+/+}$ cells maintaining higher viability than their knockout counterparts, however are not significant (Figure 8). Overall, the NCI-N87 *CDH1*$^{-/-}$ /*CDH1*$^{+/+}$ cell culture analysis has validated Entinostat as a potential SL compound, and is consistent with previous drug screening in MCF10A cells [47].

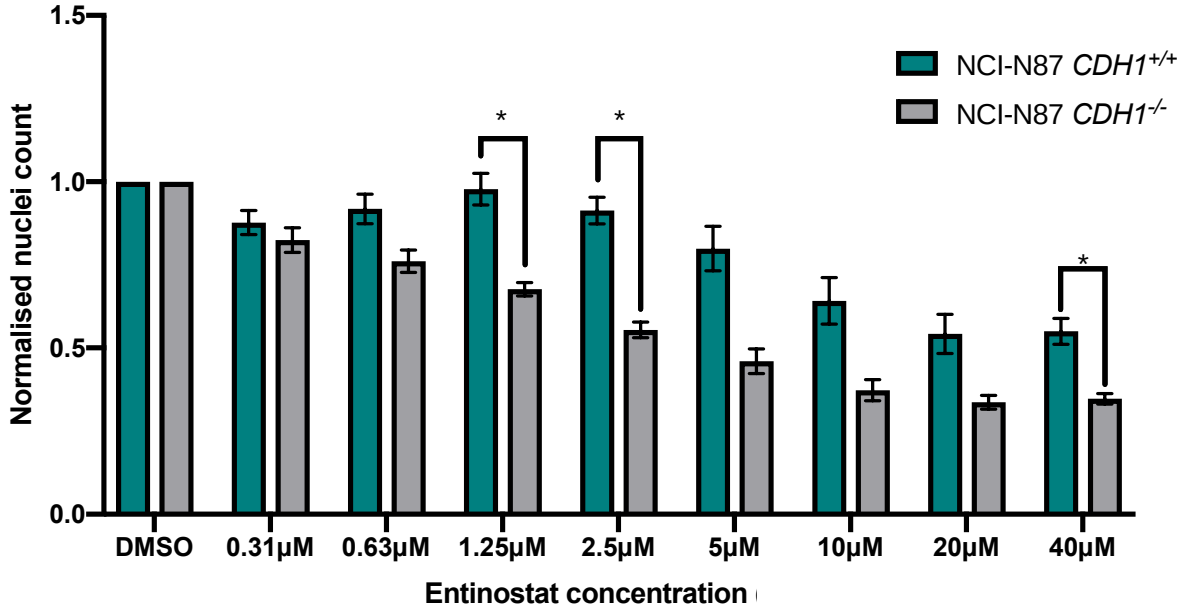

Figure 8: Normalised nuclei counts 48 hours post treatment with a serial dilution of Entinostat.
An isogenic pair of NCI-N87 cells used: CDH1$^{+/+}$ *(green bars) and CDH1*$^{-/-}$*(grey bars). Cells were treated with a serial dilution of* Entinostat*, ranging from 0.31 µM - 40 µM.* A significant synthetic lethal response was seen in NCI-N87 CDH1$^{-/-}$ cells at 1.25µM, 2.5µM and 40µM. *µM = micro molar. Data represents averaged values of three biological replicates with standard error shown. Holm-Sidak adjusted p-values calculated using student's t-test *P<0.05; **P<0.01,***P<0.001.*

4.1.2.2. Pracinostat

NCI-N87 cells were treated for 48 hours with a serial dilution of Pracinostat, with concentrations ranging from 0.31 µM to 40 µM, according to the protocol described in methods section 3.2. Pracinostat showed a significant SL effect at concentrations of 0.31, 0.63, 1.25 and 20 µM, p-values of 0.006, 0.003 and 0.014, and 0.038 respectively (Figure 9). All other Pracinostat concentrations showed an SL trend, with *CDH1*$^{+/+}$ cells maintaining higher viability than the *CDH1*$^{-/-}$, however these were not statistically significant. Treatment

with ≥1.25 µM Pracinostat strongly decreased the viability of both cell lines (Figure 9). Although some concentrations within this range show significant SL, a 50% decrease in viability of *CDH1*$^{+/+}$ cells, representing healthy gastric cells, would clearly be harmful to the patient.

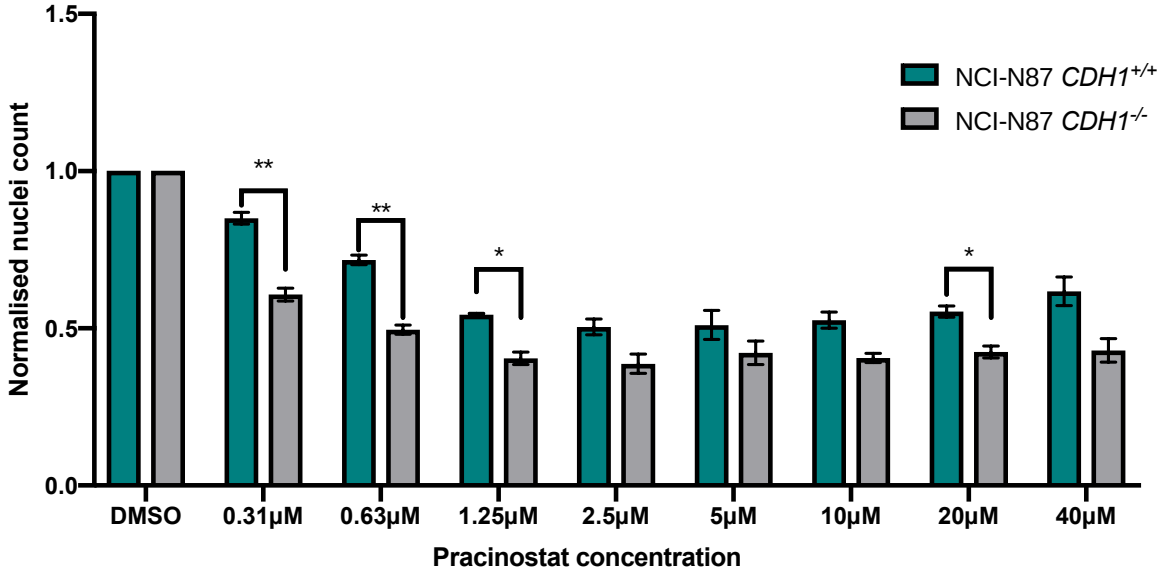

Figure 9: Normalised nuclei counts 48 hours post treatment with a serial dilution of Pracinostat.
An isogenic pair of NCI-N87 cells used: CDH1$^{+/+}$ *(green bars) and CDH1*$^{-/-}$*(grey bars). Cells were treated with a serial dilution of* Pracinostat*, ranging from 0.31µM - 40 µM. A significant synthetic lethal response was seen in NCI-N87 CDH1*$^{-/-}$ *cells at concentrations including and below 1.25µM, and at 20*µM*. µM = micro molar. Data represents averaged values of three biological replicates with standard error shown. Holm-Sidak adjusted p-values calculated using student's t-test *P<0.05; **P<0.01,***P<0.001.*

4.1.2.3. Mocetinostat

Mocetinostat demonstrated the most significant SL effect compared to all other compounds assessed in this project, with every concentration showing a significantly decreased viability (p-value <0.05) in *CDH1*$^{-/-}$ cells relative to *CDH1*$^{+/+}$ (Figure 10). Results were done in triplicate according to the aforementioned protocol. Highly significant results were seen at the 10µM an 40 µM concentrations, both having an adjusted p-value of 0.0089. The significant synthetic lethal effect seen at concentrations of ≤ 1.25 µM (adjusted p-values

0.006, 0.003, 0.014) is particularly encouraging since the *CDH1*$^{+/+}$ cell viability is unaffected, while the *CDH1*$^{-/-}$ cell viability has decreased by 20-30%. At concentrations above 1.25 µM, the viability of both cell lines decreases (Figure 10). In a clinical context, potential chemopreventative compounds will need to have a minimal impact on *CDH1*$^{+/+}$ cells, to minimise side effects on the patient. Lower concentrations of Mocetinostat are therefore preferable as the *CDH1*$^{+/+}$ cell viability is unaffected.

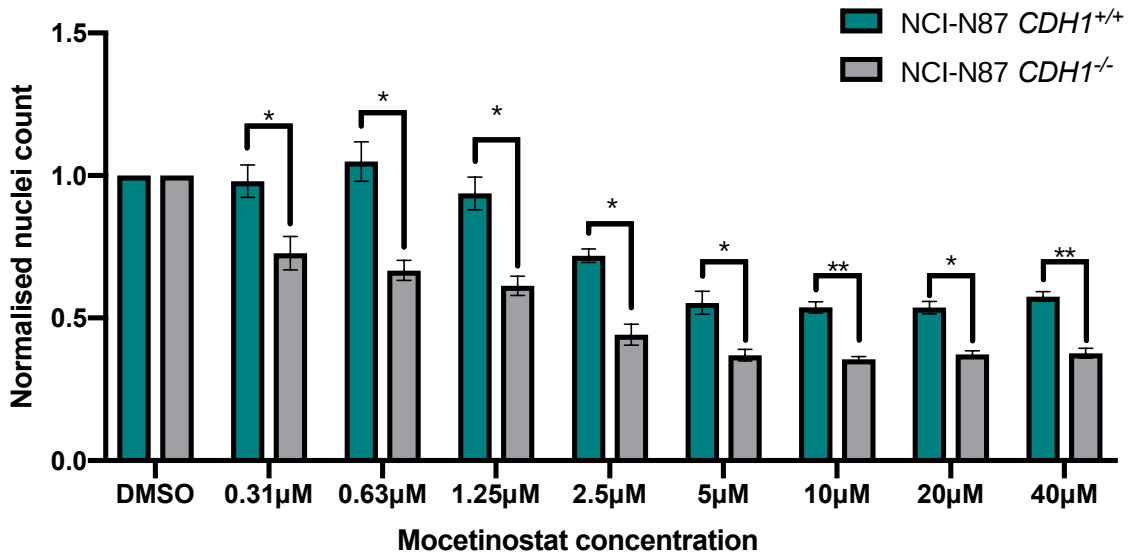

Figure 10: Normalised nuclei counts 48 hours post treatment with a serial dilution of Mocetinostat.

An isogenic pair of NCI-N87 cells used: CDH1$^{+/+}$ *(green bars) and CDH1*$^{-/-}$ *(grey bars). Cells treated with a serial dilution of* Mocetinostat*, ranging from 0.31 µM - 40 µM. A synthetic lethal response was seen in NCI-N87 CDH1*$^{-/-}$ *cells at all concentrations. Data represents averaged values of three biological replicates with standard error shown. Holm-Sidak adjusted p-values calculated using student's t-test *P<0.05; **P<0.01,***P<0.001.*

4.1.2.4. Vorinostat

Vorinostat is the final drug tested in the NCI-N87 model, cells were treated for 48 hours with a serial dilution of Vorinostat, with concentrations ranging from 0.31 µM to 40 µM. Vorinostat showed a significant SL effect at a concentration of 1.25 µM with an adjusted p-value of 0.035 (Figure 11). The 2.5 µM and 5 µM concentrations also display an inhibition of

CDH1$^{-/-}$ cells compared to the WT, however not significant. All other concentrations maintained a minor SL trend, with *CDH1*$^{+/+}$ cells having a slight higher viability than their knockout counterparts (Figure 11).

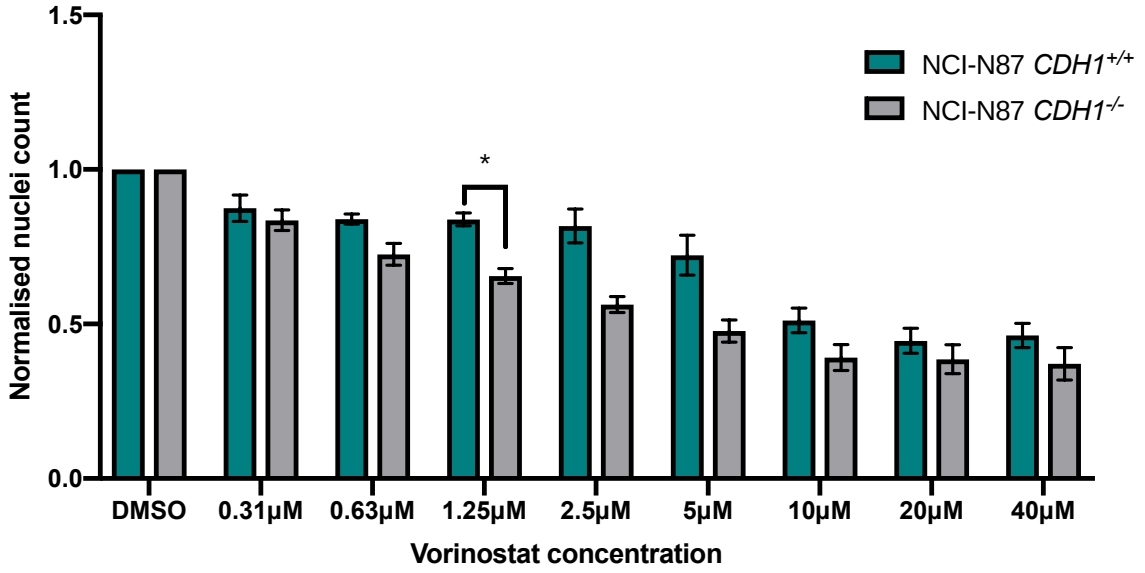

Figure 11: Normalised nuclei counts 48 hours post treatment with a serial dilution of Vorinostat.
An isogenic pair of NCI-N87 cells used: CDH1$^{+/+}$ *(green bars) and CDH1*$^{-/-}$*(grey bars). Cells were treated with a serial dilution of* Vorinostat*; 0.31µM - 40 µM. A modest synthetic lethal response was seen at 1.25µM In NCI-N87 CDH1*$^{-/-}$ *cells. Data represents averaged values of three biological replicates with standard error shown. Holm-Sidak adjusted p-values calculated using student's t-test *P<0.05; **P<0.01,***P<0.001.*

4.2. ALI Organoid data

The ALI gastric organoid model is a medium throughput 3D model of gastric cancer. ALI organoids develop from neonate mouse gastric stem cells, leading to differentiation into spherical structures made up of all gastric cell lineages. Organoids are grown in a collagen matrix containing a co-culture of myofibroblasts, at an air-liquid interface [66]. Although organoids are a lower throughput model compared to the NCI-N87 cell model, organoids are a more representative of the *in vivo* gastric environment, therefore more beneficial and informative screening tool. The ALI organoid culture model and drug assay was optimised previously based off the Ootani *et al.* protocol, in the cancer genetics lab by Yasmin Nouri

and Tanis Godwin [66]. In this section, two drugs screened in the NCI-N87 cell line, Mocetinostat and Vorinostat were further validated in the ALI organoids.

4.2.1. ALI drug screening

ALI organoids were generated from murine gastric tissue and cultured for two days prior to drug addition. To develop the *CDH1*$^{-/-}$ organoids, knockout of *CDH1* was induced by endoxifen on day zero. Organoids were then treated with drug for four days. Organoid area was measured on day 2 (day of drug addition) and day 6 (final day of assay) (Figure 12) using FIJI and the growth rate calculated. This was used as a comparative measure of viability. The concentrations of Vorinostat and Mocetinostat used in the ALI model were based off the NCI-N87 data (results sections 4.1.2.3 and 4.1.2.4).

The percentage change in growth measurement was used to analyse viability of the ALI organoids and to identify any SL effect (Figure 13). To find this, area was measured for each organoid on day 2, before drug addition, and on day 6, after 4 days exposed to drug. Area measurements were done manually using FIJI. Area data was then logged and subtracted to find the log change in growth. Log form of area data was used so that analysis was done in additive scale and error bars could be calculated. A log scale also accounts for variation in organoid sizes and number. Growth rates for each drug treatment group were normalised to the corresponding DMSO control (*CDH1*$^{+/+}$ or *CDH1*$^{-/-}$ control).

DMSO percentage change in growth is displayed as 100 (dotted line) on the graph (Figure 13). Data is not statistically significant, as the confidence intervals for the *CDH1*$^{+/+}$ and *CDH1*$^{-/-}$ for each treatment showed complete overlap, therefore no statistical test was done.

Data were anti-logged to present as a percentage scale relative to DMSO. Statistical analysis of was undertaken in consultation with Associate Professor Mik Black.

4.2.1.1. Vorinostat

Vorinostat was chosen to be taken through into the ALI model as it showed a significant SL effect in 2D cell culture, and is also already FDA approved for the treatment of haematological cancers [62]. Therefore it is a promising compound if an SL effect is present, as prior understanding of safety and toxicity will allow for approval of future clinical trial and treatment production for HDGC. ALI organoids were treated for four days with 5 µM of Vorinostat as per the protocol described in the methods section 3.2. This 5 µM concentration was chosen as previous data from Vorinostat treatment of ALI organoids showed that no response was seen at lower concentrations [74]. Three biological replicates were completed, representative images of organoids treated with Vorinostat and DMSO control are shown in Figure 12.

Control organoids were treated with DMSO. Uninduced *CDH1*$^{+/+}$ DMSO treated organoids (Figure 12A) showed a normal growth rate from day 2 to day 6, and a healthy morphology consisting of a transparent spherical structure with an intact outer wall of gastric cells. Induced *CDH1*$^{-/-}$ organoids treated with DMSO presented with the same phenotype, clear lumen and no signs of necrotic cells, indicating no effect on organoid viability from endoxifen treatment.

After four days of 5 µM Vorinostat treatment, both uninduced (*CDH1*$^{+/+}$) and induced (*CDH1*$^{-/-}$) organoids had a similar phenotype to the DMSO treatment group, as intact spheres of transparent tissue (Figure 12A & B). More images of Vorinostat treated organoids can be

seen in Appendix 1. The data shows that 5 µM of Vorinostat has not had a visible effect on organoid viability. This suggest that a higher concentration of Vorinostat will need to be tested to translate the SL effect seen in cell culture into the ALI model.

Vorinostat treatment in the ALI organoids also showed no SL effect in percentage change in growth (Figure 13). Change in growth between *CDH1*$^{+/+}$ and *CDH1*$^{-/-}$ organoids were similar and there was a slight increase in growth compared to DMSO (100) (Figure 13). There was considerable variation in both size and number of Vorinostat treated organoids, with a range of 3-17 organoids per well with different sizes. Although change in growth is an accurate measure, it is insufficient to account for all the variation. 5µM Vorinostat did not have any effect on growth rate in the *CDH1*$^{-/-}$ organoids. The concentration of Vorinostat will be increased in further experiments to try and replicate the SL effect seen in the NCI-N87 model.

4.2.1.2. Mocetinostat

Mocetinostat was further validated as an SL compound in the ALI model due to its significant SL effect at every concentration in the NCI-N87 model. Mocetinostat was originally tested at a concentration of 2.5 µM, however this concentration was lethal to both *CDH1*$^{+/+}$ and *CDH1*$^{-/-}$ organoids, so the concentration was lowered to 0.63 µM for further experiments. Mocetinostat at 0.63 µM was added to organoids at day 2 and cultured until day 6 when the viability of organoids was tested. Representative images of induced *CDH1*$^{-/-}$ and not induced *CDH1*$^{+/+}$ organoids treated with Mocetinostat are shown in Figure 12. DMSO controls are representative for both drugs, as each experiment trialled two drugs, at the same DMSO concentration, with the same gastric tissue.

Uninduced *CDH1*$^{+/+}$ organoids treated with 0.63 µM Mocetinostat had a normal growth rate and displayed no signs of death, maintaining the intact transparent phenotype (Figure 12A). However the *CDH1*$^{-/-}$ organoids displayed clear signs of death. Following drug treatment the organoid on day 6 has dark granular cells within then lumen indicating the presence of necrotic cells. There was also disintegration of the organoid wall (see for example the lower left side of the D6 treated organoid in Figure 12B. Visually the phenotypes display an SL trend, *CDH1*$^{+/+}$ organoids maintain a healthy phenotype similar to the DMSO control, while *CDH1*$^{-/-}$ organoids show signs of death.). These images indicate *CDH1*$^{-/-}$ ALI organoids treated with Mocetinostat may be more sensitive than wild type *CDH1*$^{+/+}$. Further images of organoid disintegration due to Mocetinostat treatment are in Appendix 2. To quantify the observed effect, a qualitative measurement and analysis on percentage change in growth was done.

Mocetinostat treatment, however, did indicate a difference in growth rate between the *CDH1*$^{+/+}$ and *CDH1*$^{-/-}$ organoids, although it was not significant (Figure 13). The data is suggestive of increased sensitivity of *CDH1*$^{-/-}$ organoids to treatment of 0.63 µM of Mocetinostat, compared to WT. However it will need to be further analysed through more replicates within the ALI model, or testing in an alternative model that is less prone to variation in size of the organoids.

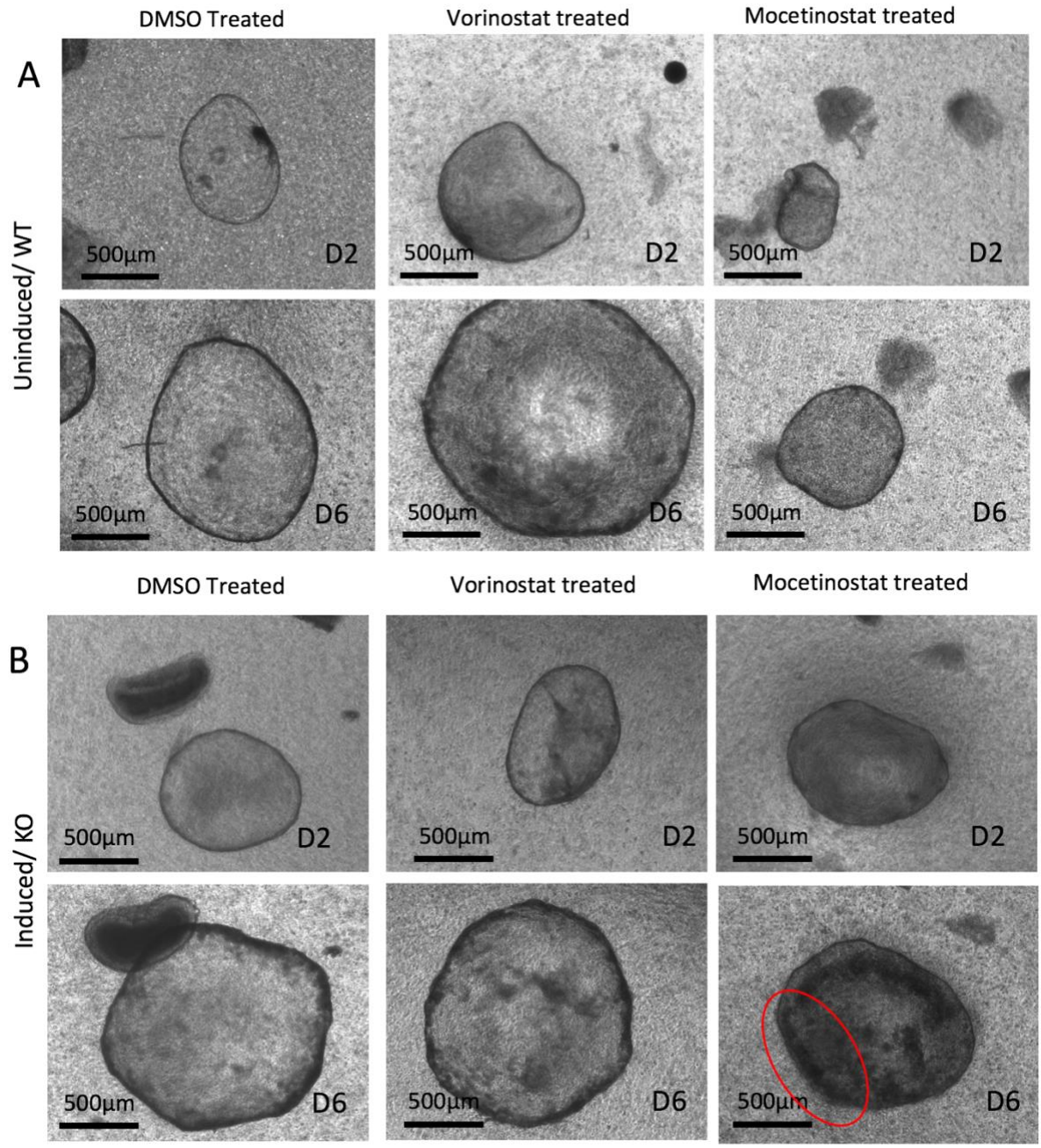

Figure 12: Representative brightfield images of Air-Liquid interface (ALI) organoids treated with DMSO (control), Vorinostat and Mocetinostat.
(A) Uninduced (Wild type) organoids on day 2 (D2) and day 6 (D6), treated with 0.1% DMSO, 5µM Vorinostat and 0.63µM Mocetinostat, exhibiting healthy growth patterns and appearance. (B) Induced (CDH1 Knockout) organoids on D2 and D6, treated with 0.1% DMSO, 5µM Vorinostat and 0.63µM Mocetinostat. DMSO and Vorinostat treated organoid are exhibiting healthy growth and appearance, Mocetinostat treated organoid showing a death phenotype (dark, grainy, disintegrating), red circle indicates an area of disintegration.

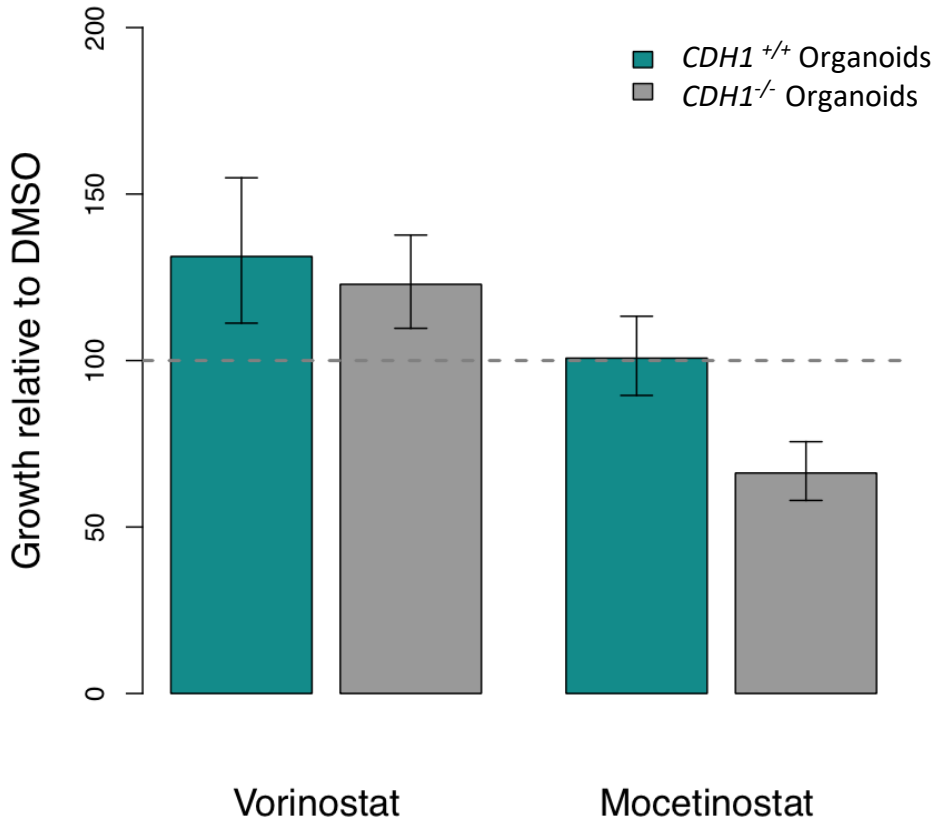

Figure 13: Percentage change in growth analysis of ALI organoids treated with Vorinostat and Mocetinostat.
Area data of day 2 and day 6 was logged and subtracted to obtain the change in growth. Data was unlogged back to a percentage scale and normalised to DMSO, indicated by the dotted line at 100% growth rate. Error bars are standard error. Green bar = CDH1$^{+/+}$ organoids and grey bar = CDH1$^{-/-}$ organoids. Graph produced in consultation with Associate Professor Mik Black.

4.2.2. 'Halo' organoids

4.2.2.1 Identification of Halo organoids

Two types of organoid growth develop in the ALI model. Firstly 'true' organoids (Figure 14A) occur where a substantial population of gastric stem cells are present in the primary tissue piece, which are able to proliferate rapidly into a spherical monolayer of epithelial cells with a clear lumen, similar to *in vivo* gastric glands. The myofibroblast co-culture supports

this growth through the release of growth factors and the collagen matrix for support of the 3D structure. True organoids were analysed for percentage change in growth and considered a true representative model of the *in vivo* gastric gland.

The other form of growth that can occur in the ALI model has been termed a 'halo' organoid, which occurs when the primary tissue remains within the proliferative cells and a ring of organoid tissue surrounds the primary tissue. The true cystic organoid structure does not form as the primary tissue remains to support the proliferative cells (Figure 14B). These are termed 'halo' organoids as the proliferative growth around the primary tissue looks like a floating halo. These structures grow when there likely aren't enough stem cells in the tissue, the tissue is too large to be degraded or growth factors secreted by the myofibroblasts were not sufficient. Approximately 15-20 of these structured were present per well. Imaging of these 'halo' structures was performed to better understand organoid development and to see if the impact of the drugs on these structures was different to the true organoids.

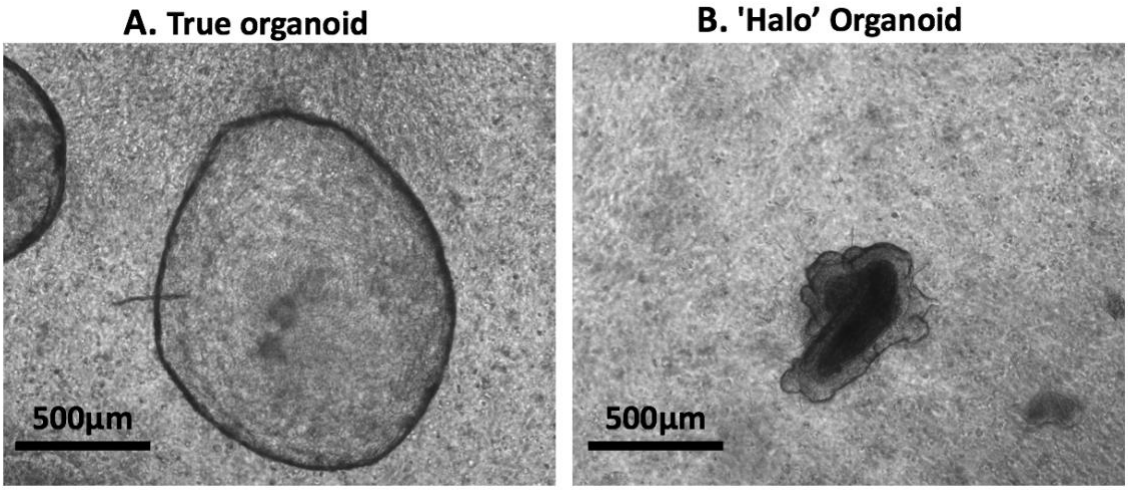

Figure 14:Comparative image of a true organoid compared to a 'halo' organoid.
(A)True organoid, clear cystic structure, clear lumen with no residual primary tissue. (B)'Halo' organoid, primary tissue clearly visible as black centre with proliferative growth surrounding.

The ALI drug assay was completed after day 6, when the final area measurement was taken. However, it was noticed that the halo organoids started to disintegrate on day 6 in the *CDH1*$^{-/-}$ wells treated with drug. To understand this interesting artefact and see if there was a differential effect occurring in these structures (*CDH1*$^{-/-}$ vs. WT), halo organoids were further imaged until day 12 to determine the impact of the drug over a longer term. Media was changed every three days but no further drug was added. Figure 15 shows the comparison of *CDH1*$^{+/+}$ and *CDH1*$^{-/-}$ halo organoids treated with Vorinostat on day 6 and then day 12. The halo for the *CDH1*$^{+/+}$ organoid has remained intact (Figure 15A) while the *CDH1*$^{-/-}$ organoid treated with Vorinostat has disintegrated, there is no halo left surrounding the primary tissue (Figure 15B). To quantify this observation, a blinded assay on halo integrity was then carried out to investigate whether a differential effect could be seen in these structures following treatment with both Vorinostat and Mocetinostat.

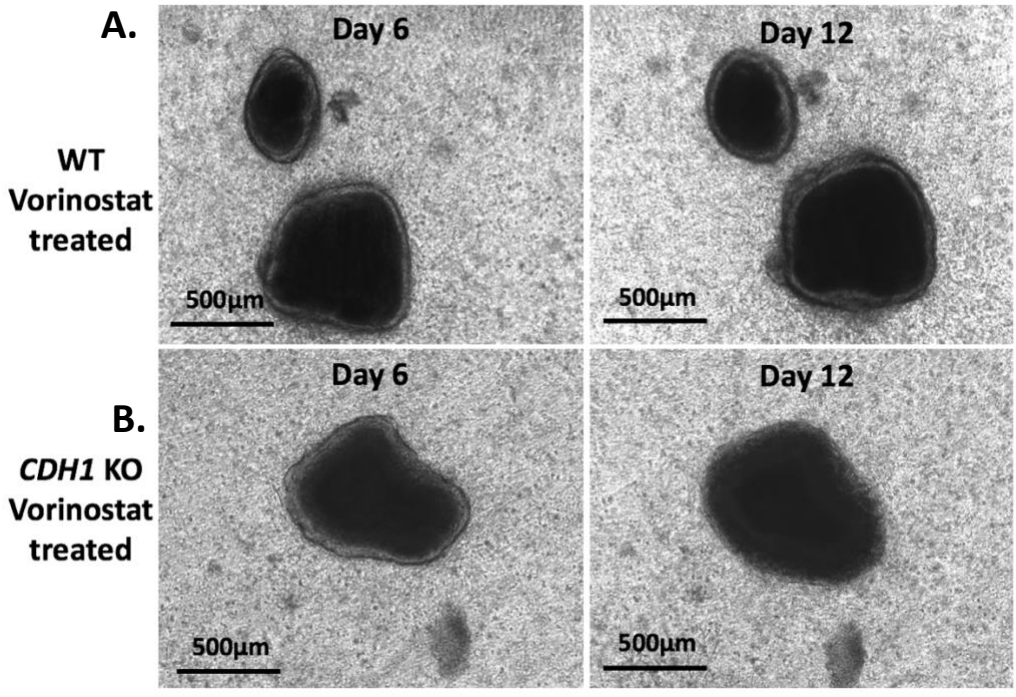

Figure 15: Representative images of halo degradation in 5µM Vorinostat treated ALI organoids. *(A) CDH1*$^{+/+}$ *halo organoid on day 6 and day 12 treated with 5 µM Vorinostat. Halo surrounding primary tissue has remained intact over the 6 days of growth. (B) CDH1*$^{-/-}$ halo organoid on day 6 and day 12 treated with *5µM Vorinostat. Halo surrounding primary tissue has degraded by day 12.*

4.2.2.2. Halo organoid analysis

85 halo organoid images from day 12 were blinded and then analysed for halo integrity. Analysis of each image was done by at least two individuals (not the author). Images were removed of all labels and renamed alphabetically and randomised, then individuals were asked to score halo integrity or disintegration. If an image had a difference in integrity score it was further analysed by two other individuals. Figure 16 shows the data from the blinded analysis. A minimum of 10 halo organoids are in each treatment group. DMSO treated halos present a similar percentage of disintegrated organoids in both *CDH1*$^{+/+}$ and *CDH1*$^{-/-}$ groups. With around 80-90% of the halos remaining intact. Vorinostat *CDH1*$^{+/+}$ halos are similar to DMSO with around 80% remaining intact, *CDH1*$^{-/-}$ Vorinostat treated had just over 60% of halos remain intact, which is a slight SL trend. However, Mocetinostat halo organoids demonstrated a strong SL effect with 100% of the *CDH1*$^{-/-}$ organoids being classified as disintegrated, while over 60% in the *CDH1*$^{+/+}$ group remained intact (Figure 16). This assay was only completed once due to time constraints. Results from this assay were similar to that of the true organoid growth rate analysis. This is an interesting result that will need to be further replicated and the halo organoids characterised to understand the artefact occurring.

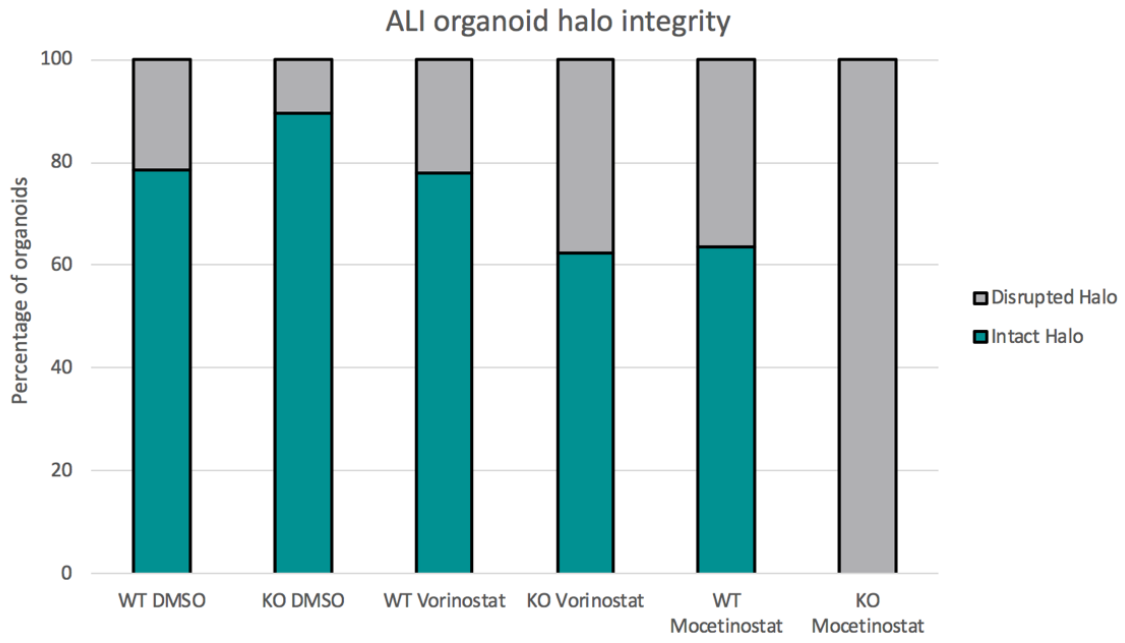

Figure 16: ALI halo organoid integrity blinded analysis.
Green bars indicate Intact halos and grey indicates a disrupted halo. WT are organoids have functional CDHI. KO are organoids which have been induced with endoxifen and CDH1 has been knocked out.

In summary, the ALI model has provided a valuable 3D model to investigate further the *in vivo* SL capabilities of Vorinostat and Mocetinostat. The analysis in the ALI model has shown that the SL trend of Mocetinostat seen in NCI-N87 culture, is also a trend in the ALI organoids, both within the true organoids and the halo organoids. Variation within the ALI model has meant data has been difficult to process, and significance hard to define. Overall SL trends are able to be observed, but the variability of the ALI model has precluded firm conclusions. For this reason we investigated a second organoid model – the submerged model.

4.3. Submerged organoid data:

The third phase of this project is the optimisation of a new organoid model, submerged organoids, in order to develop a higher throughput, more consistent organoid model for SL

drug screening. The submerged model was originally established in the Clevers laboratory, and involves organoids being grown within a Matrigel matrix and fully submerged in growth factor-enriched media [65, 68]. Some of the limitations discovered with the ALI model are able to be overcome with the submerged organoids. Fresh gastric tissue is not required for each experiment, as they are able to be passaged. This is less time consuming and means the model is higher throughput. Secondly, the variation in size and organoid number seen with the ALI model organoids can be avoided as the submerged organoids are seeded as individual cells, which can be counted and all grow into similar size organoids.

Prior to the start of this project, many of the culture conditions and protocol for the submerged organoid model had been established by Tom Brew based on the protocols from the Clevers laboratory[65, 68]. As per ALI organoids, there is the same inducible *CDH1*$^{-/-}$ knockout model for the submerged organoids. This phase of the project involved optimisation of specific conditions for the submerged model, investigation into the addition of a TGFß inhibitor, seeding density analysis for the drug protocol and lastly looking into the DMSO toxicity of these organoids. Followed by, a pilot Mocetinostat drug assay completed. More replicates of the drug assay could not be done in the time frame of this project.

4.3.1. TGFßi addition to growth media

During propagation culture of the submerged organoids, certain organoids would develop an adhered phenotype with budding growths, rather than the spherical organoids which are representative of the gastric gland. This was hypothesised to be a form of epithelial to mesenchymal transition (EMT). TGFß is known to be related to the cause of EMT due to its upregulation of WNT signalling which activates EMT [75]. TGFß is a component of the Matrigel used for the submerged organoid culture, however concentration of the protein

varies per batch. A higher TGFß concentration could lead to more EMT organoids and a redundant drug assay. Although not always present in submerged organoid media [65], the addition of a TGFß inhibitor (TGFßi) is a factor in some gastric submerged organoid preparations. For example Bartfeld *et al*. add 10µM to complete growth medium and show regular spherical organoid growth [68]. Therefore addition of a TGFßi was trialled.

Organoids were cultured for six days and imaged through brightfield microscopy to see the impact of TGFßi in the media. TGFßi was added to complete growth media on day 0 and then continuously for all media changes (every 3 days) and compared to the same complete growth media without TGFßi, also changed every three days. Figure 17 is a representative organoid image from each treatment group on day 2 and day 6 of the assay. The organoids grown in regular growth medium have a normal phenotype on day 3 with a transparent spherical structure, however by day 6 these organoids have had a complete phenotype change. Organoids in normal media on day 6 adhere to the base of the growth plate, have lost their spherical structure, display budding growths, and are releasing cells outwards into the Matrigel, indicative of an EMT phenotype(Figure 17). Comparatively the organoids grown in TGFßi containing growth medium display normal spherical structure on both day 2 and day 6. The organoids have normal growth rates and have no signs of death (granulation, disintegration, blackening)(Figure 17). Therefore all submerged organoid complete growth media will now contain TGFßi at 2µM concentration. This avoids the risk of TGFß in the Matrigel causing EMT and creating organoids that are no longer representative of the *in vivo* gastric system, and therefore not a relevant model for drug screening. TGFßi addition to growth medium maintains spherical gastric organoids which are appropriate for the modelling of HDGC.

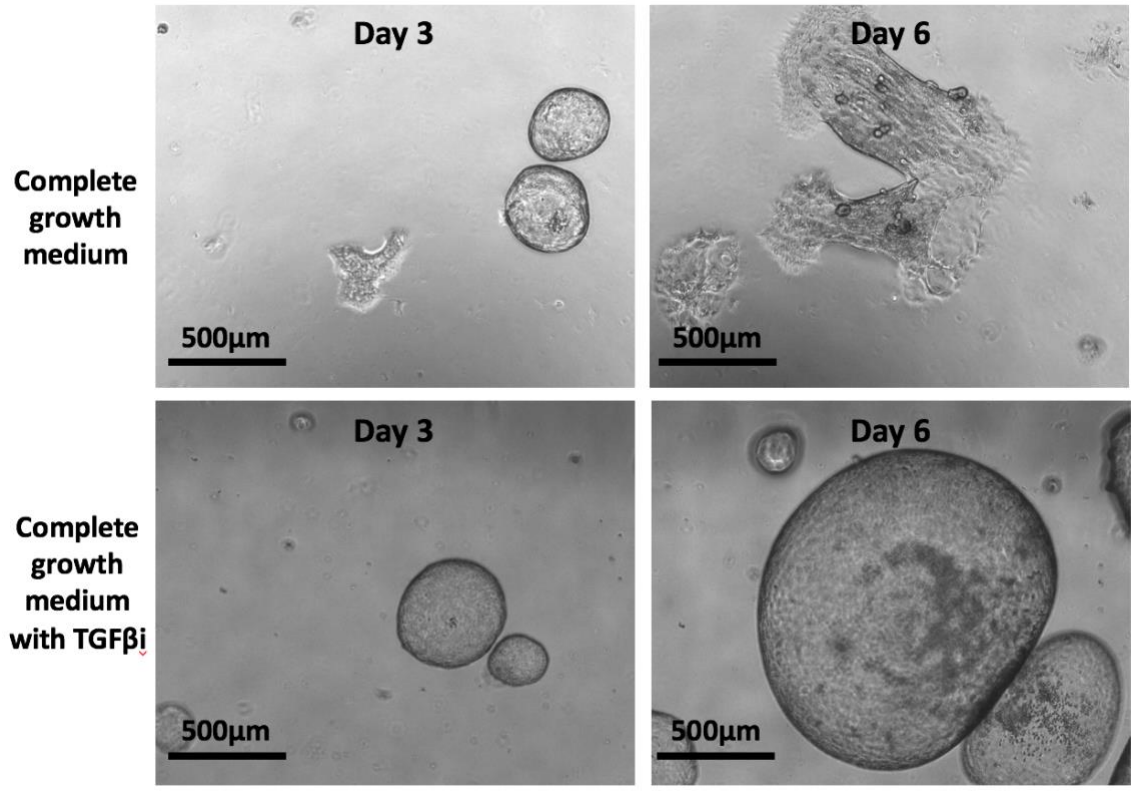

Figure 17: Submerged organoids treated with and without TGFß inhibitor.
Top: Submerged organoids grown in complete growth media, on day three and day six. Can see the EMT-like phenotype on day 6. Bottom: Submerged organoids grown in complete growth medium containing TGFß inhibitor. On both day three and day six, a healthy spherical morphology and normal growth is seen on both days.

4.3.2. Seeding density analysis

It was necessary for future drug assays in the submerged model to be completed within 96 well cell culture plates to allow for multiple concentrations of drugs to be tested at once, similarly to 2D cell culture. However, submerged organoids had previously only been grown in 24 well plates in our laboratory. Therefore, an analysis of seeding density was done to find the optimum number of organoids that could be grown per well.

Rather than a dome of Matrigel in the centre of the well, as done in 24 well plates, 96 well plates have the entire base of the well coated in Matrigel that the organoids grow within. The submerged organoids were seeded as single cells, as this allows accurate seeding as cells are able to be counted, and similar size organoids all originate from one cell. Previous data from

our laboratory has shown that the lower the seeding density the more variation in organoid number, so the highest number of submerged organoid cells seeded with minimal organoid degradation was wanted.

In Figure 18, it is clear that a seeding density of 5000 single cells per well is too high and overcrowding is having an effect on organoid viability. By day four, organoids are showing signs of death, the organoids are darkening which indicates necrotic cells and the growth rate is slow as organoids look a similar size to that of day 2 in culture. There are also some organoids which have disintegrated (Figure 18). In comparison, a seeding density of 1000 cells has organoids which are displaying no signs of death. On day 4 of culture they have a normal growth rate, a clear lumen free of necrotic cells, and the outer border of cells is intact. Therefore a seeding density of 1000 cells was taken through into the drug assay. At this density, there are enough organoids growing to reduce effect of variability, they display a healthy appearance and their size is regular.

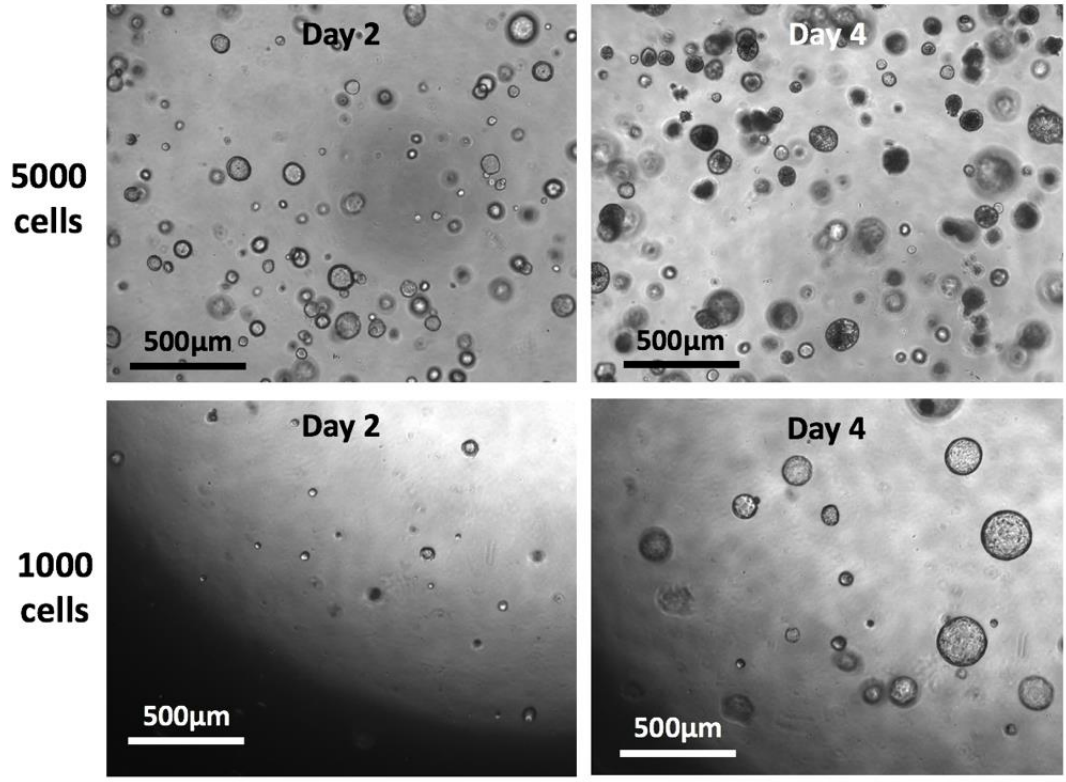

Figure 18: Representative images of submerged organoid seeding density analysis. *Submerged organoids seeded at different densities to optimise drug assay. Top- 5000 cells per well, day four showing dark organoids with very little growth. Bottom- 1000 cells per well, day four displaying healthy submerged organoids.*

4.3.3 DMSO toxicity

Finding the concentration of DMSO that is toxic to the submerged organoids was the next step in the optimisation of the drug assay. Drug compounds and endoxifen are reconstituted in DMSO, therefore it is essential to know at what concentration of DMSO organoid viability is affected. Submerged organoids were seeded at the optimal 1000 cells per well and treated with increasing concentrations of DMSO and left for 48 hours. Viability of organoids was tested using the Alamarblue assay and read on the CLARIOstar. All concentrations below 0.2% DMSO had similar viability, between 6-8 thousand fluorescence intensity , indicating very little impact of DMSO on the organoids (Figure 19). The concentration of DMSO which is added for each drugging assay is normally below 0.05%, therefore this data shows that there should be very little impact on the organoids from the 0.05% DMSO the drugs are

reconstituted in; toxicity should not be present until concentrations greater than 0.2% (Figure 19). There was variability in this data so replicates need to be done. It is also essential that this DMSO toxicity is also tested in induced *CDH1* knockout organoids, but this could not be completed for this thesis due to time constraints.

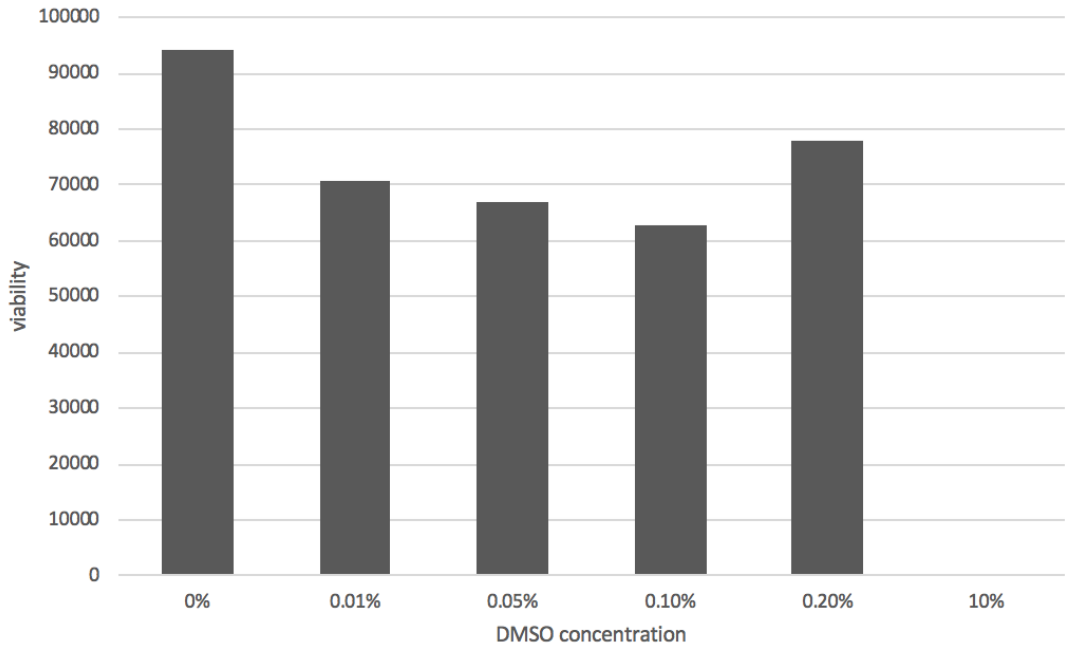

Figure 19: Submerged organoid DMSO toxicity assay.
Triplicate technical replicates for each concentration of DMSO. Viability is a normalised total fluorescence, analysed through AlamarBlue assay, read through the CLARIOstar. Similar viability for concentrations of DMSO 0.01%-0.2%. Toxicity only seen at the DMSO concentration of 10%.

4.3.4 Preliminary submerged model drug assay

A pilot drugging experiment was carried out to identify any other issues that may need to be optimised. Mocetinostat was used as it showed the most promising SL effect in both the NCI-N87 and ALI organoid data. Only one biological replicate could be done due to time constraints.

Submerged organoids were seeded in Matrigel at 1000 single cells per well in a 96 well plate. Organoid *CDH1* knockout was induced after 24 hours, and then after a further 24 hours Mocetinostat was added at increasing concentrations - 1.25 µM, 2.5 µM, 5 µM and a DMSO control. Organoids were treated with Mocetinostat for 48 hours, and then stained with AlamarBlue and viability read as normalised total fluorescence, on the CLARIOstar plate reader. Results were in triplicate for each concentration. Columns in the bar graph (Figure 20) are an average normalised to DMSO. The 2.5 µM concentration of Mocetinostat showed a promising differential trend, with the wildtype $CDH1^{+/+}$ maintaining viability same as the DMSO control (Figure 20). In contrast the $CDH1^{-/-}$ organoids had a greater than 20% decrease in viability. Although more replicates will need to be done to validate this result, this data is further suggestive of $CDH1^{-/-}$ organoids being more sensitive to Mocetinostat than WT organoids (Figure 20). This assay is also still in development and further changes are being made to make results obtained more accurate (see discussion for further detail).

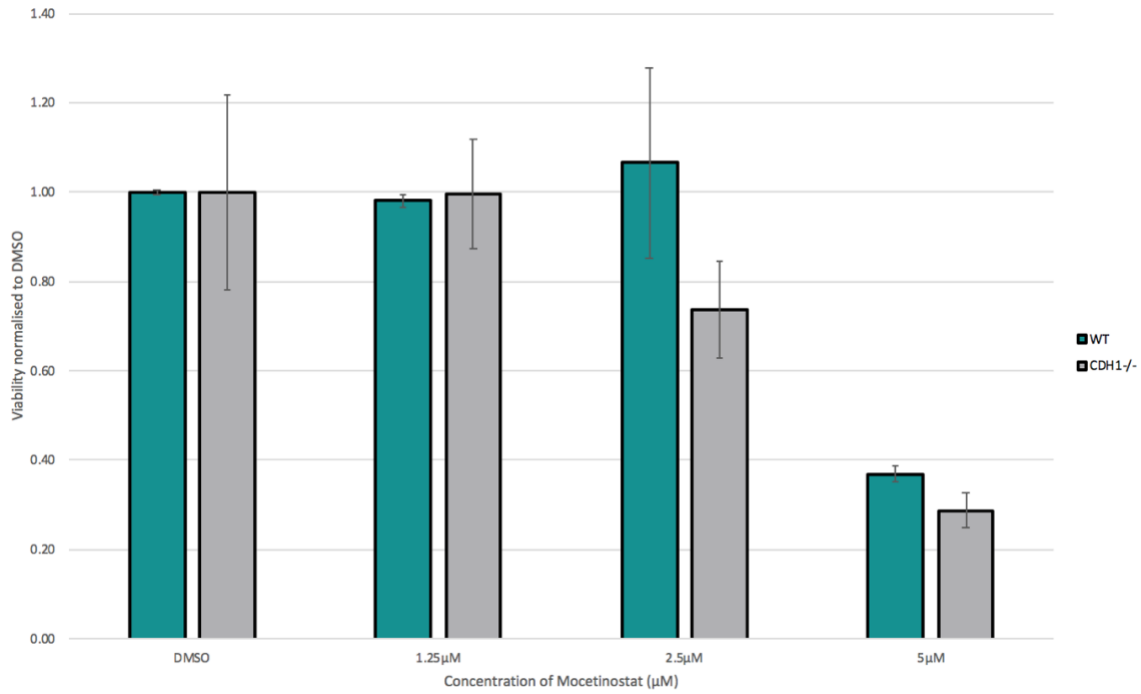

Figure 20: Submerged organoids pilot drug assay with Mocetinostat
Green: WT CDH1$^{+/+}$, Grey: KO *CDH1*$^{-/-}$. AlamarBlue viability assay of submerged organoids treated with Mocetinostat at a range of concentrations normalised to DMSO. Error bars are standard error.

4.4. Concluding remarks

Synthetic lethal compounds have been identified and validated in the three models in this project. Firstly in the NCI-N87 drug screen, all compounds exhibited an SL response, with *CDH1*$^{-/-}$ cells having consistent lower viability than the WT counterparts (Figure 7-11). Atorvastatin showed a synthetic lethal trend at higher concentrations, (Figure 7) but no significant differential in viability between *CDH1*$^{+/+}$ and *CDH1*$^{-/-}$ cells was observed. Of all the compounds, Mocetinostat exhibited the greatest SL effect, as at every concentration there was a significant decrease in viability of the *CDH1*$^{-/-}$ cells compared to WT.

From this initial model, Vorinostat and Mocetinostat were then validated in an ALI organoid model. Results from the ALI drug assay were not conclusive due to limitations in the drug screening protocol. However Mocetinostat still displayed a difference in viability between *CDH1*$^{-/-}$ and *CDH1*$^{+/+}$ organoids, indicative of a possible SL trend.

The optimisation of the submerged model was successful, allowing for a pilot drug screen with Mocetinostat to be completed. The SL trend seen in previous models was again present, where *CDH1*$^{-/-}$ organoids displayed a lower viability compared to *CDH1*$^{+/+}$ when treated with Mocetinostat. Through analysis of all three models together, this project has successfully identified Mocetinostat as a potential synthetic lethal chemopreventative compound for the treatment of HDGC.

Chapter 5: Discussion

5.1 Identification of SL compounds

The NCI-N87 cell culture model, ALI organoid model and the submerged organoid model, have been useful tools in this project for the identification of synthetic lethal compounds which selectively inhibit *CDH1*$^{-/-}$ cells. Compounds tested in this project, Atorvastatin, Entinostat, Pracinostat, Vorinostat and Mocetinostat were chosen as they were identified in the original known drug screen carried out in our laboratory [47]. From the preliminary NCI-N87 high-throughput screen of these five compounds, data was used to decide which compounds to investigate further in the organoid models. This was based on greatest SL effect and analysis of current clinical trial data.

5.1.1 Vorinostat

Vorinostat is a pan-HDACi which has been FDA approved for the treatment of cutaneous T-cell lymphoma (CTCL) [61]. Similarly to Mocetinostat, adverse effects of Vorinostat described in section 1.3.1.2, are able to be therapeutically managed so the drug has minimal impact on the patient.

Initial testing in the NCI-N87 model of HDGC, Vorinostat showed a statistically significant synthetic lethal differential effect in *CDH1*$^{-/-}$ cells over the *CDH1*$^{+/+}$ cells at a concentration of 1.25 µM. Other concentrations of Vorinostat displayed a synthetic lethal trend with *CDH1*$^{-/-}$ cells consistently having a lower viability compared to the *CDH1*$^{+/+}$ cells. Vorinostat was chosen for testing in the ALI organoid model, due to the FDA approval status, and low risk of severe adverse effects. This prior FDA approval in CTCL would allow for a quicker

pipeline for the FDA approval of Vorinostat for any other cancer type, for example for the treatment of HDGC.

Vorinostat was further validated in the ALI organoid model for the drug-induced selective inhibition of *CDH1*$^{-/-}$ cells. The data shows no SL effect for Vorinostat at 5 μM with the phenotype (Figure 12B) and change in growth being equivalent to that of the DMSO control (Figure 13). A higher concentration of Vorinostat may need to be tested to replicate the SL effect seen in the cell culture model to a 3D model. The variability in the ALI model meant that area change data had a very widespread distribution and therefore the effect or lack of effect of the drug is not easily understood from initial replicates. Secondly since the ALI model is a low throughput model, multiple concentrations of drug were not able to be tested at once. These limitations were resolved through the submerged model, discussed further below.

Previous research has shown that Vorinostat treatment upregulates E-cadherin expression and is protective in cancer development. While this is not a mechanism for the synthetic lethal effect seen, it may be protective of development of HDGC. The singular functional *CDH1* gene that mutation carriers have could be upregulated through Vorinostat treatment, to prevent the formation of cancerous phenotypes forming [76].

5.1.2. Mocetinostat

Mocetinostat is an HDACi which specifically inhibits class 1 and 4 HDAC's. Through current clinical trial data, it has been shown that Mocetinostat does have certain adverse effects, as described in section 1.3.1.2., however these have been able to be minimised

therapeutically [59]. FDA approval exists for Mocetinostat as treatment for diffuse large cell B lymphoma [60].

Mocetinostat demonstrated a significant SL effect at every concentration tested, with decreased viability in *CDH1*$^{-/-}$ cells relative to *CDH1*$^{+/+}$ cells (Figure 10). This data for Mocetinostat is particularly encouraging because at the three lowest concentrations, *CDH1*$^{+/+}$ cell viability is unaffected, while *CDH1*$^{-/-}$ cell viability drops to 70% viable. Mocetinostat concentrations demonstrating no impact on viability of the *CDH1*$^{+/+}$cells represents unaffected 'healthy' cells. This is promising for a potential HDGC therapy, because treatment with minimal impact on the patient is preferable. The significant SL effect observed across multiple drug concentrations was the reason that Mocetinostat was selected for further validation in the other HDGC models in this project.

In contrast to Vorinostat, Mocetinostat did show a difference in viability in the ALI organoid model, with signs of organoid death compared to the 'healthy phenotype of the DMSO negative control organoids (Figure 12). The data for change in growth for organoids treated with Mocetinostat was also suggestive of a minor differential effect, with a slight inhibition of growth in *CDH1*$^{-/-}$ organoids compared to *CDH1*$^{+/+}$ organoids. This data was not statistically significant and only suggestive of a SL response, showing more investigation needs to occur in other models. Although both drugs were tested in triplicate, with each replicate containing at least three organoids, the data is extremely variable, indicated by the large standard error of the mean (Figure 13).

Finally, Mocetinostat was trialled in the submerged organoid model. This drug assay was a pilot assay, because the submerged model is not yet fully optimised, however, a synthetic

lethal effect was seen in this singular replicate. At a concentration of 2.5 µM Mocetinostat, the *CDH1*$^{+/+}$ organoids had 100% viability compared to the DMSO control, while the *CDH1*$^{-/-}$ organoids dropped in viability to around 70% compared to the DMSO control. This pilot assay with Mocetinostat provided important information for the further development of the viability assay in the submerged organoid model. Once optimisation is complete, the submerged model will be used for future drug screening of potential SL compounds.

Mocetinostat displayed selective inhibition of *CDH1*$^{-/-}$ cells across three different models of HDGC. This is hypothesised to be due to Mocetinostat specifically inhibiting HDAC1, which is overexpressed in 68% of gastric cancers [56]. Vorinostat and Pracinostat are pan-HDAC inhibitors, meaning they inhibit all classes of HDAC. This nonspecific inhibition likely effects the viability of both the *CDH1*$^{+/+}$ cells and *CDH1*$^{-/-}$ cells, leading to a decreased SL effect [52]. Mocetinostat has also been shown to increase E-cadherin and B-catenin localisation to the membrane, which reduces the EMT phenotype. This may be another potential mechanism of Mocetinostat inhibiting in cancer formation, as cells are inhibited from undergoing EMT [77].

5.2. Limitations

5.2.1 NCI-N87 model

One limitation of the NCI-N87 drug screening protocol used is the measurement of cell viability. Viability was measured through total nuclei counting, Hoechst stains the nuclei, which can then be counted and a differential nuclei count between *CDH1*$^{+/+}$ cells and *CDH1*$^{-/-}$ cells observed. This method does not establish whether the difference in cell number is due to a cytostatic or cytotoxic effect. Hoechst stain is able to diffuse across cell membranes, staining both live and dead cells and all are counted for the final nuclei count [78]. Drug

treatment could cause a decrease in *CDH1-/-* cell number through a cytostatic mechanism, where cells are live but inhibited from completing the cell cycle and unable to replicate. The other option is that drug treatment has a cytotoxic effect by killing *CDH1-/-* cells. The mechanism of drug action could be either cytostatic or cytotoxic, as Hoechst is not able to differentiate between the two. For a potential chemopreventative treatment, a drug which inhibits *CDH1-/-* cell growth needs to be cytotoxic, to completely eliminate cancer cells, and thus any risk of HDGC. To address this, apoptosis assays need to be carried out with the drugs used in this study prior to further pre-clinical development (see future directions).

5.2.2. ALI model

The ALI model is designed to be similar to the *in vivo* gastric gland. Organoids are grown at an air-liquid interface within a collagen matrix, facilitating growth of 3D structures. Co-cultures with MFB represents the *in vivo* stromal cells. Resulting organoids are made up of all lineages of gastric cells. All of these features make the ALI model theoretically suitable as a pre-clinical model. However, in practice, these characteristics are also what make the ALI model variable and not an ideal model for drug screening.

Several sources of variability were observed in ALI organoids. Firstly, variability in the size of the organoids in every well was problematic. This variation in size is introduced due to the fragmentation of gastric tissue in the preparation of organoids. Gastric tissue is mechanically broken down with scissors, and although the protocol is strictly followed, tissue of varying sizes will always be produced. When seeded, the larger pieces of tissue generally form larger organoids, while smaller tissue fragments form smaller organoids. Secondly, there was variation in the number of organoids per well. This is introduced as the number of tissue pieces cannot be counted. It is assumed that they are evenly distributed throughout the collagen preparation and this mixture is then evenly distributed across each well. This leads

to the variability in the number of organoids per well, from 3 – 20 growing in a single experiment preparation. Lastly, variation is introduced by certain tissues developing classic organoids and others forming halo organoids. This may be due to differences in stem cell abundance across different pieces of tissue. Tissue containing more stem cells is likely able to develop into a true organoid, with limited stem cell populations forming halo organoids. The halo organoid growth may also be due to the myofibroblasts surrounding the piece of tissue not releasing enough growth factors to stimulate organoid growth. Halo organoids are not representative of the *in vivo* gastric gland, therefore they cannot be analysed alongside true organoids to determine drug effect on growth. A separate analysis of halo organoids was performed in this project (Figure 16). Overall for the ALI model to be an effective model for drug screening, it requires tissue pieces to be of uniform size, with an equal concentration of tissue placed into each well, and most of these equal sized pieces of tissue to form into true organoids. These factors cannot be controlled using the current protocol, therefore this model is not suitable for routine drug screening in its current format. However it does provide a useful model for the visualisation of *CDH1*-null cells in HDGC, as it is the most representative model of the *in vivo* gastric gland. After drug treatment, confocal microscopy of the ALI organoids remains an important step in understanding the impact of drug on cellular structure, behaviour and how the overall organoid structure is impacted.

5.2.3 Submerged

The submerged model was developed in the Clevers laboratory [65, 68], and is being adapted in the Cancer Genetics Laboratory by Tom Brew. The organoids grown in the laboratory have similar growth and phenotype to those seen in the literature.

Optimisation of the submerged model started in an attempt to circumvent some of the limitations previously discussed with the ALI model. For example, the ALI model is low throughput as it requires fresh murine gastric tissue for each preparation. The submerged model allows for organoids to be propagated, with murine gastric tissue only being required for the initial preparation. This makes submerged organoids a medium throughput model which is easier to use for the preparation of drug screening assays. Secondly the co-culture with myofibroblasts is no longer required, as the growth factors added to the complete culture medium stimulate growth of the organoids (Table 2). For each ALI drug assay preparation, 14 confluent 75 mL cell culture flasks of myofibroblasts were required to be added to the collagen. The addition of growth factors to the culture medium is a less labour intensive process, another factor that makes the submerged model higher throughput compared to the ALI model.

As discussed, the variability in size, number and type of organoid in the ALI model is the major limitation of that model for drug screening. The submerged model is able to avoid all of these issues. Submerged organoids are seeded in the Matrigel as single cells and all follow a similar growth pattern, so at day six are all a similar size, this can be seen in the seeding density analysis (Figure 18). As submerged organoids are propagated as single cells, they are also able to be counted on the LUNA automated cell counter, so the concentration of cells in the volume of Matrigel is known and accurate seeding occurs (Figure 18). Lastly, as tissue is only used for the initial preparation, halo organoids are not present in the submerged model. However, the EMT phenotype organoids were an uncharacterised structure that was not-representative of the *in vivo* environment, although these EMT like structures were able to be inhibited with the TGFßi. treatment (Figure 17). The submerged model is therefore better for drug screening, as it is far less variable that the ALI.

5.3 Future directions

A Fluorescence Activated Cell Sorting (FACS) apoptosis assay could be used to distinguish between a cytotoxic or cytostatic effect upon drug treatment. The FACS assay uses fluorescent markers to distinguish between live, early apoptotic and late apoptotic cells. The first marker, Annexin-V-FITC protein binds to pre-apoptotic membrane proteins which are present on the outside of a cell about to undergo apoptosis [79]. The second marker propidium iodide selectively diffuses into apoptotic or necrotic cells due to a compromised cell membrane. FACS separates the sample into three populations. Viable cells are negative for both markers, early apoptotic cells are only Annexin-V-FITC positive, and late apoptotic cells are positive for both Annexin-V-FITC and Propidium iodide. A cytotoxic drug will result in pre-apoptotic and late-apoptotic cell population, whereas a cytostatic drug will maintain viable cells. This would allow for differentiation between cytostatic and cytotoxic compounds [79]

The current analysis of organoid viability is done through brightfield imaging and area measurement. This analysis is therefore done using one 2D image of a 3D spherical structure. This method just analyses size, however organoids are viable growths, that require a more in depth and accurate measure of viability. The representative images of the ALI organoids show this issue with all displaying similar growth rates, however some are much unhealthier looking than the DMSO controls (Appendix 1, 2 & 3). A growth rate analysis may notice very little change, but a viability assay looks into the more accurate measure of cells which are actually viable. A viability assay would be able to distinguish between organoids made up of viable cells compared to necrotic cells, regardless of size of the organoid, and be a better measure of any SL effect.

Another future direction for this model is to look at the long term impacts on the organoids of drug treatment. The 12 day analysis of the halo organoid data showed that long term Mocetinostat had a strong SL effect (Figure 13). This long term analysis could be applied to the ALI true organoids, which have been shown to be able to be cultured for a year [80]. This could potentially have a more definitive selective inhibition of *CDH1*$^{-/-}$ organoids, especially if multiple doses of drug were added, similarly to a treatment scheme for how patients would take the medication as chemoprevention. It would be interesting to complete an assay with long term multiple dosage of organoids to see if *CDH1*$^{+/+}$ organoids would remain viable while *CDH1*$^{-/-}$ organoids slowly disintegrate, similarly to the halo organoids (Figure 16).

TGFßi. treatment removed the EMT phenotype organoids from the preparation, however for drug screening assays it may interfere with the drug treatments, as the inhibitor is currently added with every new media addition every three days. A future experiment looking into adding the TGFßi on only day 0 when the organoids are seeded, to see whether one dose is enough to inhibit the EMT phenotype would be valuable. It could then be confirmed that any selective decrease in viability of *CDH1*$^{-/-}$ organoids is due to the compound being tested alone, not a combination of the compound and the TGFßi.

Secondly, the DMSO toxicity test of the submerged organoids needs to be further validated. The preliminary analysis completed in this project demonstrated that the *CDH1*$^{+/+}$ organoids did not experience a significant decrease in viability in concentrations of DMSO below 0.2%. Further investigation into what concentration of DMSO is the maximum before toxicity occurs needs to be done, and a replicate of this experiment with *CDH1*$^{-/-}$ organoids is essential. Following on from the assay optimisation, the submerged organoid model will be utilised for medium throughput SL drug screening in a 3D organoid model. Initially with

more replicates of Mocetinostat, as the pilot study in this model, will be done to confirm the SL effect seen due to Mocetinostat in the submerged organoids.

5.4. Clinical relevance

A chemopreventative compound for the treatment of HDGC is necessary as the current optimal treatment is prophylactic gastrectomy. Gastrectomy has both physical and psychological impacts on patients and is also overtreatment in cases where there is no family history of gastric cancer but a *CDH1* mutation present. A chemopreventative compound will aim to target *CDH1* negative cells to reduce the risk of HDGC development, and therefore the need for prophylactic gastrectomy.

The drugs chosen for this project were specifically assessed for low toxicity and minimal adverse effects to minimise the impact on patients. As a potential preventative therapy, carriers of *CDH1* mutations do not have gastric cancer and are physically healthy, therefore a chemopreventative drug should not impact day to day life with severe adverse effects, and make carriers unwell, as that is not an improvement on the current treatment of prophylactic gastrectomy. For example the HDACi Mocetinostat, FDA approval exists for this compound indicating low levels of adverse effects and a pre-existing pipeline for the potential FDA approval for Mocetinostat HDGC treatment. Adverse effects associated with HDACi are fatigue, nausea and diarrhoea, which are all effects that can be managed therapeutically. Drug data was analysed for each compound to find concentrations where $CDH1^{+/+}$ cells exhibit close to 100% viability and $CDH1^{-/-}$ cell viability was significantly affected. As at significant concentrations like this, where the $CDH1^{+/+}$ cells represent healthy gastric cells, which are unaffected, leading to minimal effects on the patient.

5.5 Concluding statement

In conclusion, this project has successfully identified synthetic lethal compounds which selectively inhibit *CDH1*$^{-/-}$ cells. All compounds tested in the NCI-N87 cell culture model displayed evidence of synthetic lethality, with HDACi having the most significant selective *CDH1*$^{-/-}$ cell inhibition. Vorinostat and Mocetinostat, were further validated in an ALI organoid model. Results from the ALI drug assay were inconclusive due to limitations in the drug screening protocol. This lead to the optimisation of an alternative organoid model, referred to as the submerged organoid model, and a pilot drug assay in this model. Results from each of these model systems has successfully identified Mocetinostat as a potential chemopreventative compound for the treatment of HDGC. In future, further validation of Mocetinostat will need to be completed, in the new submerged organoid model and then in HDGC mouse models, to provide basis for a clinical trial of a chemopreventative compound for HDGC. The importance of a chemopreventative option is especially important in NZ. As the proportion of *CDH1*$^{-/-}$ mutations in the Māori population is three to five fold higher to that of the NZ European population [26]. A treatment option is necessary that eliminates the need for prophylactic gastrectomy and ultimately, the risk of development of HDGC.

Appendix

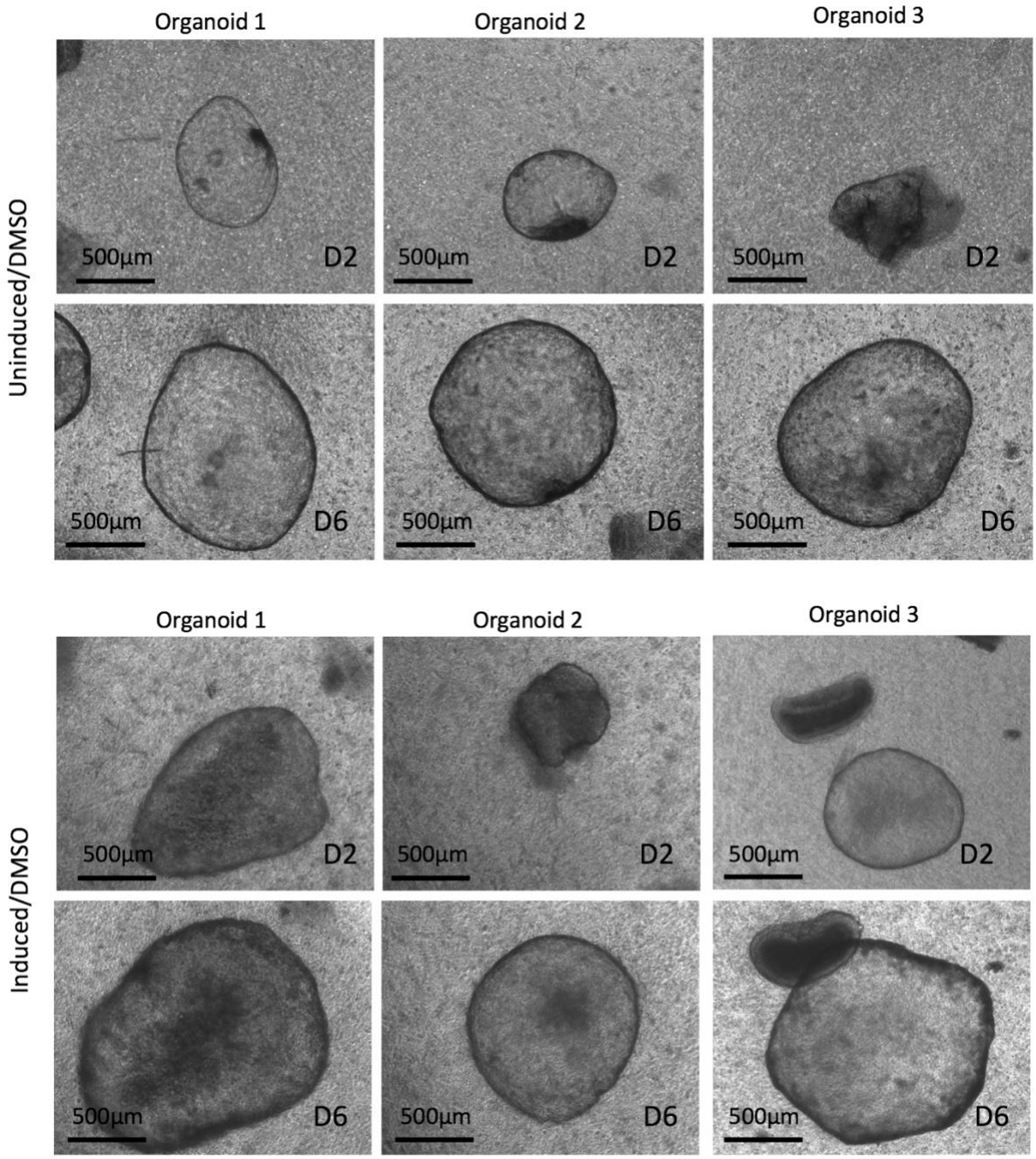

Appendix 1: Representative brightfield images of WT and CDH1 KO ALI organoids treated with the DMSO control.
Organoids shown on day 2 and day 6. All display healthy morphology.

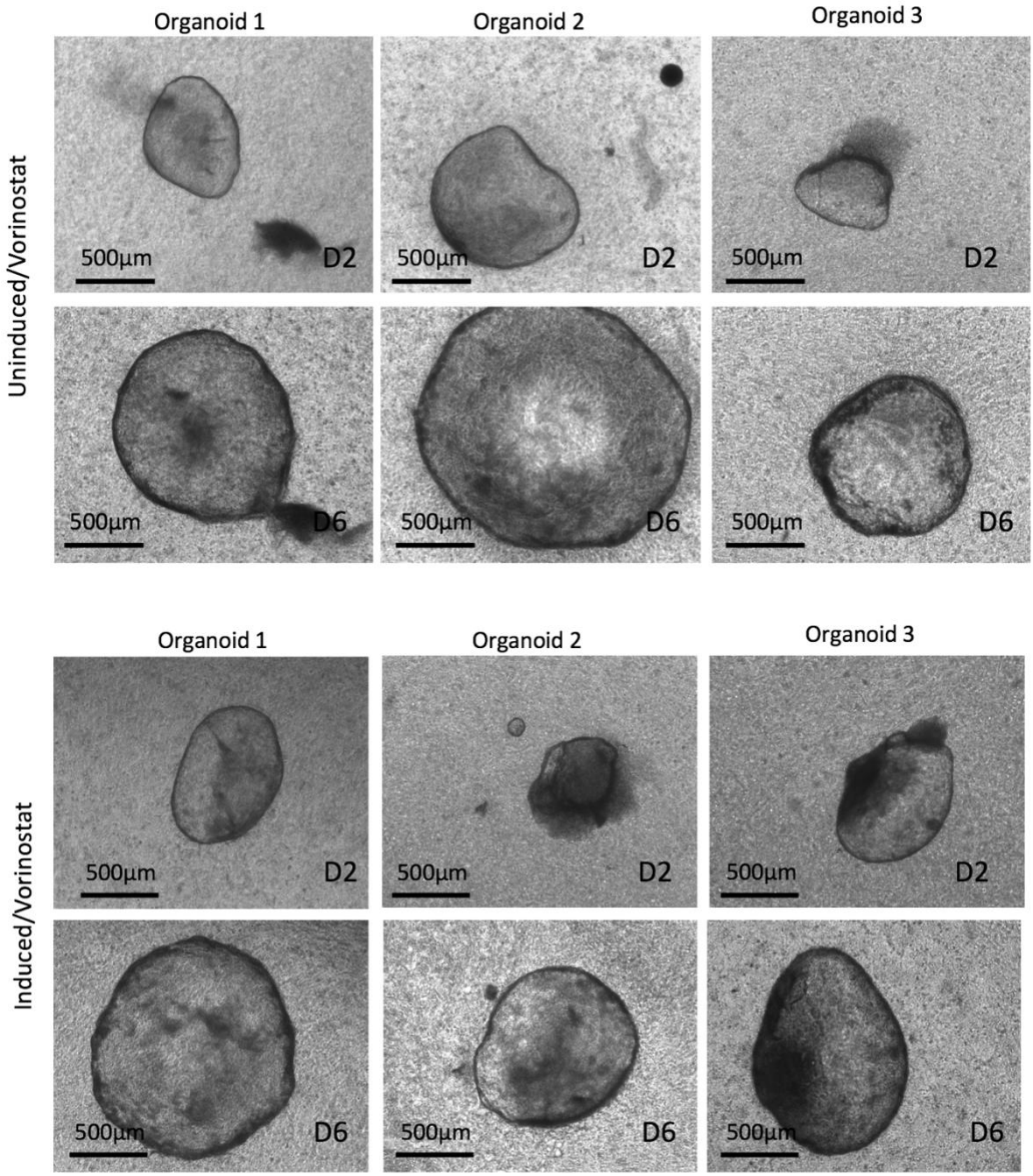

Appendix 1: Representative brightfield images of WT and CDH1 KO ALI organoids treated with 5µM Vorinostat.
Organoids shown on day 2 and day 6. All display healthy morphology.

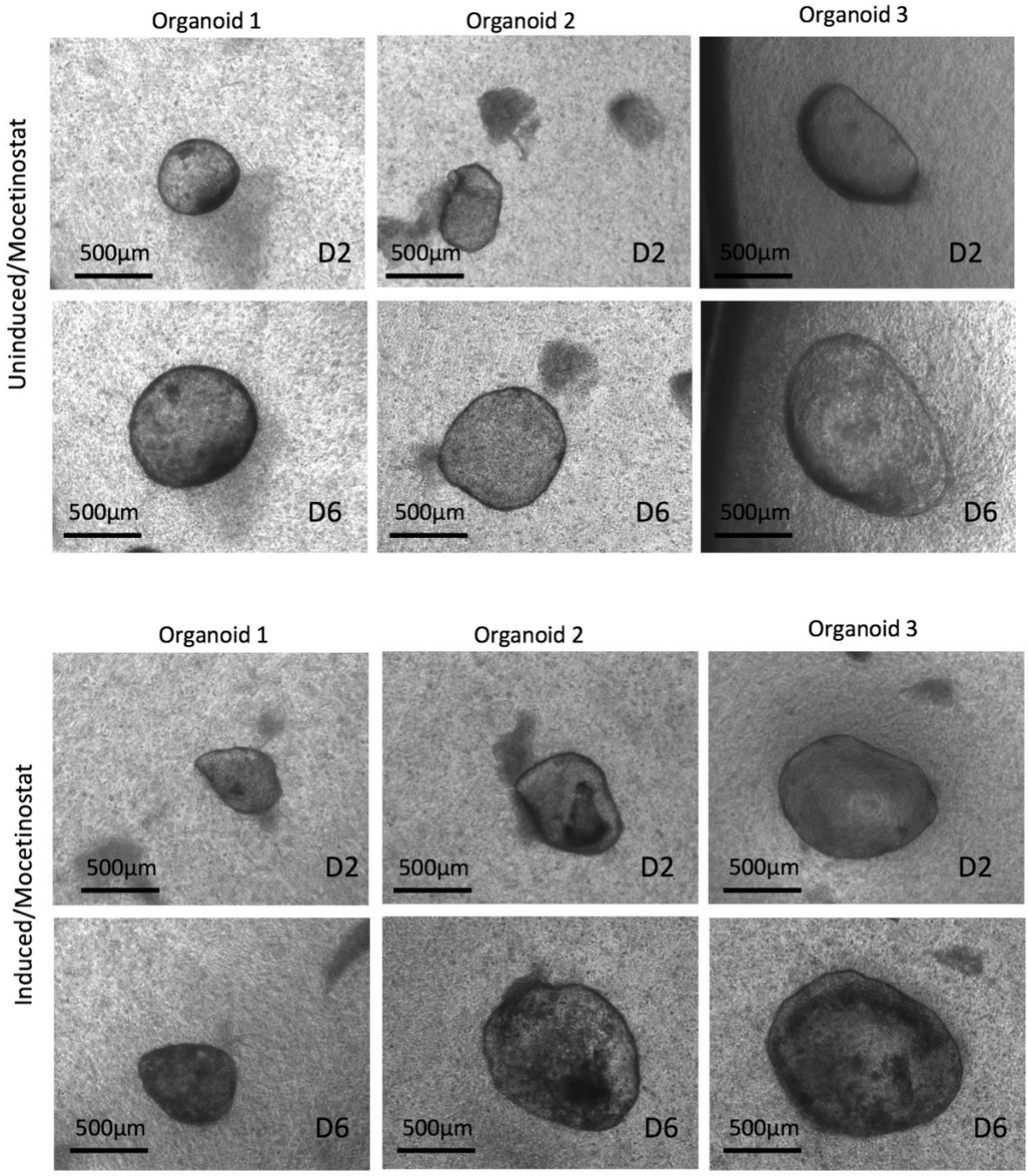

Appendix 2: Representative brightfield images of WT and CDH1 KO ALI organoids treated with the 0.63 µM Mocetinostat.

Organoids shown on day 2 and day 6. All display signs of death by day 6. Organoids are blackening, disintegrating and do not show a normal growth rate.

References:

1. Kobielak, A. and E. Fuchs, *Alpha-catenin: at the junction of intercellular adhesion and actin dynamics.* Nat Rev Mol Cell Biol, 2004. **5**(8): p. 614-25.
2. Ferlay, J., et al., *Estimating the global cancer incidence and mortality in 2018: GLOBOCAN sources and methods.* International Journal of Cancer, 2019. **144**(8): p. 1941-1953.
3. Bray, F., et al., *Global cancer statistics 2018: GLOBOCAN estimates of incidence and mortality worldwide for 36 cancers in 185 countries.* CA: A Cancer Journal for Clinicians, 2018. **68**(6): p. 394-424.
4. Poultsides, G. and J.A. Norton, *Hereditary Diffuse Gastric Cancer*, in *Gastric Cancer: Principles and Practice*, V.E. Strong, Editor. 2015, Springer International Publishing: Cham. p. 251-254.
5. Jemal, A., et al., *Global cancer statistics.* CA Cancer J Clin, 2011. **61**(2): p. 69-90.
6. Bertuccio, P., et al., *Recent patterns in gastric cancer: a global overview.* Int J Cancer, 2009. **125**(3): p. 666-73.
7. Zamani, M., et al., *Systematic review with meta-analysis: the worldwide prevalence of Helicobacter pylori infection.* Alimentary Pharmacology & Therapeutics, 2018. **47**(7): p. 868-876.
8. Uemura, N., et al., *Helicobacter pylori Infection and the Development of Gastric Cancer.* New England Journal of Medicine, 2001. **345**(11): p. 784-789.
9. Sheh, A., et al., *17(lowercase beta)-estradiol and Tamoxifen prevent gastric cancer by modulating leukocyte recruitment and oncogenic pathways in Helicobacter pylori-infected INS-GAS male mice.* Cancer Prevention Research, 2011: p. canprevres.0219.2011.
10. Karimi, P., et al., *Gastric cancer: descriptive epidemiology, risk factors, screening, and prevention.* Cancer Epidemiol Biomarkers Prev, 2014. **23**(5): p. 700-13.
11. Ang, T.L. and K.M. Fock, *Clinical epidemiology of gastric cancer.* Singapore medical journal, 2014. **55**(12): p. 621-628.
12. Oliveira, C., R. Seruca, and C. Caldas, *Genetic screening for hereditary diffuse gastric cancer.* Expert Review of Molecular Diagnostics, 2003. **3**(2): p. 201-215.
13. Hartgrink, H.H., et al., *Gastric cancer.* Lancet (London, England), 2009. **374**(9688): p. 477-490.
14. Brooks-Wilson, A.R., et al., *Germline E-cadherin mutations in hereditary diffuse gastric cancer: assessment of 42 new families and review of genetic screening criteria.* Journal of Medical Genetics, 2004. **41**(7): p. 508.
15. Ellison-Loschmann, L., et al., *Risk of stomach cancer in Aotearoa/New Zealand: A Māori population based case-control study.* PloS one, 2017. **12**(7): p. e0181581-e0181581.
16. Dockerty, J.D., et al., *Stomach cancer in New Zealand: time trends, ethnic group differences and a cancer registry-based case-control study.* Int J Epidemiol, 1991. **20**(1): p. 45-53.
17. Lauren, P., *The two Histological Main Types of Gastric Carcinoma: Diffuse and So-Called Intestinal-Type Carcinoma. An Attempt at a Histo-Clinical Classification.* Acta Pathol Microbiol Scand, 1965. **64**: p. 31-49.
18. Jawhari, A., et al., *Abnormal immunoreactivity of the E-cadherin-catenin complex in gastric carcinoma: Relationship with patient survival.* Gastroenterology, 1997. **112**(1): p. 46-54.
19. Carneiro, F., *Classification of gastric carcinomas.* Current Diagnostic Pathology, 1997. **4**(1): p. 51-59.

20. Hamilton, S.R. and L.A. Aaltonen, *WHO classification of tumours. Pathology and genetics of tumours of the digestive system.* Geneva: World health organization, 2000.
21. Hu, B., et al., *Gastric cancer: Classification, histology and application of molecular pathology.* Journal of gastrointestinal oncology, 2012. **3**(3): p. 251-261.
22. Cancer Genome Atlas Research, N., *Comprehensive molecular characterization of gastric adenocarcinoma.* Nature, 2014. **513**(7517): p. 202-209.
23. Katona, B.W. and A.K. Rustgi, *Gastric Cancer Genomics: Advances and Future Directions.* Cellular and Molecular Gastroenterology and Hepatology, 2017. **3**(2): p. 211-217.
24. Oliveira, C., et al., *E-Cadherin (CDH1) and p53 rather than SMAD4 and Caspase-10 germline mutations contribute to genetic predisposition in Portuguese gastric cancer patients.* European Journal of Cancer, 2004. **40**(12): p. 1897-1903.
25. Guilford, P., et al., *E-cadherin germline mutations in familial gastric cancer.* Nature, 1998. **392**(6674): p. 402-5.
26. Hakkaart, C., et al., *Germline CDH1 mutations are a significant contributor to the high frequency of early-onset diffuse gastric cancer cases in New Zealand Maori.* Fam Cancer, 2019. **18**(1): p. 83-90.
27. van der Post, R.S., et al., *Hereditary diffuse gastric cancer: updated clinical guidelines with an emphasis on germline CDH1 mutation carriers.* Journal of Medical Genetics, 2015. **52**(6): p. 361.
28. Guilford, P.J., et al., *E-cadherin germline mutations define an inherited cancer syndrome dominated by diffuse gastric cancer.* Hum Mutat, 1999. **14**(3): p. 249-55.
29. Oliveira, C., et al., *Germline CDH1 deletions in hereditary diffuse gastric cancer families.* Human Molecular Genetics, 2009. **18**(9): p. 1545-1555.
30. Gumbiner, B.M., *Cell adhesion: the molecular basis of tissue architecture and morphogenesis.* Cell, 1996. **84**(3): p. 345-57.
31. van Roy, F. and G. Berx, *The cell-cell adhesion molecule E-cadherin.* Cellular and Molecular Life Sciences, 2008. **65**(23): p. 3756-3788.
32. Gumbiner, B.M., *Proteins associated with with cytoplasmic surface of adhesion molecules.* Neuron, 1993. **11**(4): p. 551-564.
33. Humar, B. and P. Guilford, *Hereditary diffuse gastric cancer and lost cell polarity: a short path to cancer.* Future Oncol, 2008. **4**(2): p. 229-39.
34. Perl, A.K., et al., *A causal role for E-cadherin in the transition from adenoma to carcinoma.* Nature, 1998. **392**(6672): p. 190-3.
35. Kalluri, R. and E.G. Neilson, *Epithelial-mesenchymal transition and its implications for fibrosis.* The Journal of clinical investigation, 2003. **112**(12): p. 1776-1784.
36. Takeichi, M., *Cadherin cell adhesion receptors as a morphogenetic regulator.* Science, 1991. **251**(5000): p. 1451-5.
37. Shirayoshi, Y., T.S. Okada, and M. Takeichi, *The calcium-dependent cell-cell adhesion system regulates inner cell mass formation and cell surface polarization in early mouse development.* Cell, 1983. **35**(3, Part 2): p. 631-638.
38. Guilford, P., B. Humar, and V. Blair, *Hereditary diffuse gastric cancer: translation of CDH1 germline mutations into clinical practice.* Gastric Cancer, 2010. **13**(1): p. 1-10.
39. Hansford, S., et al., *Hereditary Diffuse Gastric Cancer Syndrome: CDH1 Mutations and BeyondHereditary Diffuse Gastric Cancer SyndromeHereditary Diffuse Gastric Cancer Syndrome.* JAMA Oncology, 2015. **1**(1): p. 23-32.
40. Charlton, A., et al., *Hereditary diffuse gastric cancer: predominance of multiple foci of signet ring cell carcinoma in distal stomach and transitional zone.* Gut, 2004. **53**(6): p. 814.

41. Nijman, S.M.B., *Synthetic lethality: general principles, utility and detection using genetic screens in human cells.* FEBS letters, 2011. **585**(1): p. 1-6.
42. Dobzhansky, T., *Genetics of natural populations; recombination and variability in populations of Drosophila pseudoobscura.* Genetics, 1946. **31**(3): p. 269-290.
43. Masel, J. and M.L. Siegal, *Robustness: mechanisms and consequences.* Trends in Genetics, 2009. **25**(9): p. 395-403.
44. Hartwell, L.H., et al., *Integrating Genetic Approaches into the Discovery of Anticancer Drugs.* Science, 1997. **278**(5340): p. 1064.
45. Farmer, H., et al., *Targeting the DNA repair defect in BRCA mutant cells as a therapeutic strategy.* Nature, 2005. **434**(7035): p. 917-921.
46. Bryant, H.E., et al., *Specific killing of BRCA2-deficient tumours with inhibitors of poly(ADP-ribose) polymerase.* Nature, 2005. **434**(7035): p. 913-917.
47. Telford, B.J., et al., *Synthetic Lethal Screens Identify Vulnerabilities in GPCR Signaling and Cytoskeletal Organization in E-Cadherin–Deficient Cells.* Molecular cancer therapeutics, 2015. **14**(5): p. 1213-1223.
48. Godwin, T.D., et al., *E-cadherin-deficient cells have synthetic lethal vulnerabilities in plasma membrane organisation, dynamics and function.* Gastric Cancer, 2018: p. 1-14.
49. Demierre, M.-F., et al., *Statins and cancer prevention.* Nature Reviews Cancer, 2005. **5**: p. 930.
50. Warita, K., et al., *Statin-induced mevalonate pathway inhibition attenuates the growth of mesenchymal-like cancer cells that lack functional E-cadherin mediated cell cohesion.* Scientific Reports, 2014. **4**: p. 7593.
51. Seveau, S., et al., *Role of lipid rafts in E-cadherin– and HGF-R/Met–mediated entry of Listeria monocytogenes into host cells.* The Journal of Cell Biology, 2004. **166**(5): p. 743.
52. West, A.C. and R.W. Johnstone, *New and emerging HDAC inhibitors for cancer treatment.* The Journal of Clinical Investigation, 2014. **124**(1): p. 30-39.
53. Fraga, M.F., et al., *Loss of acetylation at Lys16 and trimethylation at Lys20 of histone H4 is a common hallmark of human cancer.* Nature Genetics, 2005. **37**(4): p. 391-400.
54. Subramanian, S., et al., *Clinical Toxicities of Histone Deacetylase Inhibitors.* Pharmaceuticals (Basel, Switzerland), 2010. **3**(9): p. 2751-2767.
55. Mann, B.S., et al., *Vorinostat for Treatment of Cutaneous Manifestations of Advanced Primary Cutaneous T-Cell Lymphoma.* Clinical Cancer Research, 2007. **13**(8): p. 2318.
56. Choi, J.-H., et al., *Expression Profile of Histone Deacetylase 1 in Gastric Cancer Tissues.* Japanese Journal of Cancer Research, 2001. **92**(12): p. 1300-1304.
57. Knipstein, J. and L. Gore, *Entinostat for treatment of solid tumors and hematologic malignancies.* Expert Opinion on Investigational Drugs, 2011. **20**(10): p. 1455-1467.
58. Yong, W.P., et al., *Phase I and pharmacodynamic study of an orally administered novel inhibitor of histone deacetylases, SB939, in patients with refractory solid malignancies.* Annals of Oncology, 2011. **22**(11): p. 2516-2522.
59. Prince, H.M., M.J. Bishton, and S.J. Harrison, *Clinical studies of histone deacetylase inhibitors.* Clin Cancer Res, 2009. **15**(12): p. 3958-69.
60. Boumber, Y., A. Younes, and G. Garcia-Manero, *Mocetinostat (MGCD0103): a review of an isotype-specific histone deacetylase inhibitor.* Expert Opinion on Investigational Drugs, 2011. **20**(6): p. 823-829.

61. Marks, P.A. and M. Dokmanovic, *Histone deacetylase inhibitors: discovery and development as anticancer agents.* Expert Opin Investig Drugs, 2005. **14**(12): p. 1497-511.
62. Duvic, M., et al., *Phase 2 trial of oral vorinostat (suberoylanilide hydroxamic acid, SAHA) for refractory cutaneous T-cell lymphoma (CTCL).* Blood, 2006. **109**(1): p. 31-39.
63. Park, J.G., et al., *Characteristics of cell lines established from human gastric carcinoma.* Cancer Res, 1990. **50**(9): p. 2773-80.
64. Hughes, P., et al., *The costs of using unauthenticated, over-passaged cell lines: how much more data do we need?* BioTechniques, 2007. **43**(5): p. 575-586.
65. Barker, N., et al., *Lgr5+ve Stem Cells Drive Self-Renewal in the Stomach and Build Long-Lived Gastric Units In Vitro.* Cell Stem Cell, 2010. **6**(1): p. 25-36.
66. Ootani, A., et al., *An Air–Liquid Interface Promotes the Differentiation of Gastric Surface Mucous Cells (GSM06) in Culture.* Biochemical and Biophysical Research Communications, 2000. **271**(3): p. 741-746.
67. Katano, T., et al., *Gastric mesenchymal myofibroblasts maintain stem cell activity and proliferation of murine gastric epithelium in vitro.* Am J Pathol, 2015. **185**(3): p. 798-807.
68. Bartfeld, S. and H. Clevers, *Organoids as Model for Infectious Diseases: Culture of Human and Murine Stomach Organoids and Microinjection of Helicobacter Pylori.* J Vis Exp, 2015(105).
69. McCracken, K.W., et al., *Modelling human development and disease in pluripotent stem-cell-derived gastric organoids.* Nature, 2014. **516**: p. 400.
70. Lampreht Tratar, U., S. Horvat, and M. Cemazar, *Transgenic Mouse Models in Cancer Research.* Frontiers in oncology, 2018. **8**: p. 268-268.
71. Saada, J.I., et al., *Subepithelial myofibroblasts are novel nonprofessional APCs in the human colonic mucosa.* J Immunol, 2006. **177**(9): p. 5968-79.
72. Pastula, A., et al., *Three-Dimensional Gastrointestinal Organoid Culture in Combination with Nerves or Fibroblasts: A Method to Characterize the Gastrointestinal Stem Cell Niche.* Stem Cells Int, 2016. **2016**: p. 3710836.
73. Bougen-Zhukov, N., et al., *Allosteric AKT Inhibitors Target Synthetic Lethal Vulnerabilities in E-Cadherin-Deficient Cells.* Cancers, 2019. **11**(9): p. 1359.
74. Nouri, Y., *The Establishment and Characterisation of Gastric Organoids as a Model for Hereditary Diffuse Gastric Cancer* in *Biochemistry* 2019, University of Otago: University of Otago.
75. Song, J., *EMT or apoptosis: a decision for TGF-β.* Cell Research, 2007. **17**(4): p. 289-290.
76. Taylor, M.D., et al., *Combined proteasome and histone deacetylase inhibition attenuates epithelial–mesenchymal transition through E-cadherin in esophageal cancer cells.* The Journal of Thoracic and Cardiovascular Surgery, 2010. **139**(5): p. 1224-1232.e1.
77. Nural-Guvener, H.F., et al., *HDAC class I inhibitor, Mocetinostat, reverses cardiac fibrosis in heart failure and diminishes CD90+ cardiac myofibroblast activation.* Fibrogenesis & Tissue Repair, 2014. **7**(1): p. 10.
78. Cesarone, C.F., C. Bolognesi, and L. Santi, *Improved microfluorometric DNA determination in biological material using 33258 Hoechst.* Analytical Biochemistry, 1979. **100**(1): p. 188-197.
79. Chen, S., et al., *Detection of apoptosis induced by new type gosling viral enteritis virus in vitro through fluorescein annexin V-FITC/PI double labeling.* World journal of gastroenterology, 2008. **14**(14): p. 2174-2178.

80. Ootani, A., et al., *Sustained in vitro intestinal epithelial culture within a Wnt-dependent stem cell niche.* Nat Med, 2009. **15**(6): p. 701-6.
81. R Core Team (2019). *R: A language and environment for statistical computing.* R Foundation for Statistical Computing, Vienna, Austria. URL https://www.R-project.org/